

Paleoceanography and Paleoclimatology*

RESEARCH ARTICLE

10.1029/2023PA004706

Key Points:

- We evaluate the simulation of African air temperatures in Paleoclimate Modeling Intercomparison Project Phases 3 and 4 simulations of the mid-Holocene
- Energy balance decomposition analyses indicate the hydrologic cycle plays a key role in causing mid-Holocene cooling in model simulations
- “Green Sahara” experiments show that dust and vegetation affect simulated temperatures, revealing pathways for refining model simulations

Supporting Information:

Supporting Information may be found in the online version of this article.

Correspondence to:

C. Marshall,
chm2@rice.edu

Citation:





Marshall, C., Morrill, C., Dee, S., Pausata, F. S. R., & Russell, J. (2024). Causes of past African temperature change in PMIP simulations of the mid-Holocene.

Paleoceanography and Paleoclimatology, 39, e2023PA004706. <https://doi.org/10.1029/2023PA004706>

Received 28 JUN 2023

Accepted 6 APR 2024

Causes of Past African Temperature Change in PMIP Simulations of the Mid-Holocene

Charlie Marshall¹ , Carrie Morrill² , Sylvia Dee¹ , Francesco S. R. Pausata³ , and James Russell⁴

¹Department of Earth, Environmental, and Planetary Sciences, Rice University, Houston, TX, USA, ²NOAA National Centers for Environmental Information, Boulder, CO, USA, ³Centre ESCER (Etude et la Simulation du Climat a; l'Echelle Regionale) and GEOTOP (Research Center on the Dynamics of the Earth System), Department of Earth and Atmospheric Sciences, University of Quebec in Montreal, Montreal, QC, Canada, ⁴Brown University, Providence, RI, USA

Abstract Current-generation climate models project that Africa will warm by up to 5°C in the coming century, severely stressing African populations. Past and ongoing work indicates, however, that the models used to create these projections do not match proxy records of past temperature in Africa during the mid-Holocene (MH), raising concerns that their future projections may house large uncertainties. Rather than reproducing proxy-based reconstructions of MH warming relative to the Pre-Industrial (PI), models instead simulate MH temperatures very similar to or slightly colder than the PI. This data-model mismatch could be due to a variety of factors, including biases in model surface energy budgets or inaccurate representation of the feedbacks between temperature and hydrologic change during the “Green Sahara.” We focus on the differences among model simulations in the Paleoclimate Modeling Intercomparison Project Phases 3 and 4 (PMIP3 and PMIP4), examining surface temperature and energy budgets to investigate controls on temperature and the potential model sources of this paleoclimate data-model mismatch. Our results suggest that colder conditions simulated by PMIP3 and PMIP4 models during the MH are in large part due to the joint impacts of feedback uncertainties in response to increased precipitation, a strengthened West African Monsoon (WAM) in the Sahel, and the Green Sahara. We extend these insights into suggestions for model physics and boundary condition changes, and discuss implications for the accuracy of future climate model projections over Africa.

1. Introduction

Increasing temperatures in Africa over the 21st century will disrupt socioeconomic development via impacts on people, infrastructure, and biodiversity across the continent (IPCC, 2021). However, recent summaries from the Intergovernmental Panel on Climate Change report (IPCC AR5) suggest current-generation climate models have large uncertainties in regional projections for Africa. For example, under Representative Concentration Pathway (RCP) 8.5 forcing, Coupled Model Intercomparison Project (CMIP) models predict between 4 and 7.5°C of warming in tropical Africa—a vast difference in temperature for local populations (IPCC, 2013). This spread of ~3°C or more in temperature makes it difficult to quantify future climate risks incurred by extreme heat, drought and flooding, all of which may contribute to outbreaks of civil violence (Detges, 2016; Linke et al., 2018; von Uexkull, 2014; Tierney et al., 2015). The geopolitical risk to developing nations in Africa posed by climate change alone warrants efforts to reduce uncertainty in climate model estimates of future temperatures.

Paleoclimate simulations are a key tool for analyzing model behavior in response to large-scale changes in external climate forcings and different internal variability from the present. Paleoclimate proxy-model comparison has been used widely to validate climate model performance across time periods before the 20th century (Chevalier et al., 2017; Tierney et al., 2020); these efforts can provide robust benchmarks for testing model performance (Bartlein et al., 2011). Paleoclimate experiments have resulted in critical changes to model physics and parameter choices; recent salient examples include tuning of atmospheric parameters via simulating the Last Glacial Maximum (Ramos et al., 2022; P. Zhu & Zhao, 2008) and improving simulations of African climate by changing parameters related to atmospheric mixing and the vegetation moisture stress function to better simulate the “Green Sahara” (Hopcroft & Valdes, 2021; Hopcroft et al., 2021). The mid-Holocene (MH, approximately 5–8 thousand years ago) represents an important warm climate “end-member,” providing model validation tests during an inter-glacial climate with boundary conditions different from the present. During the MH in Africa, changes in orbital parameters induced wetter conditions, contributing to the so-called “Green Sahara” (see e.g. deMenocal et al. (2000); Shanahan et al. (2015); Tierney et al. (2017)). Specifically, changes in seasonal

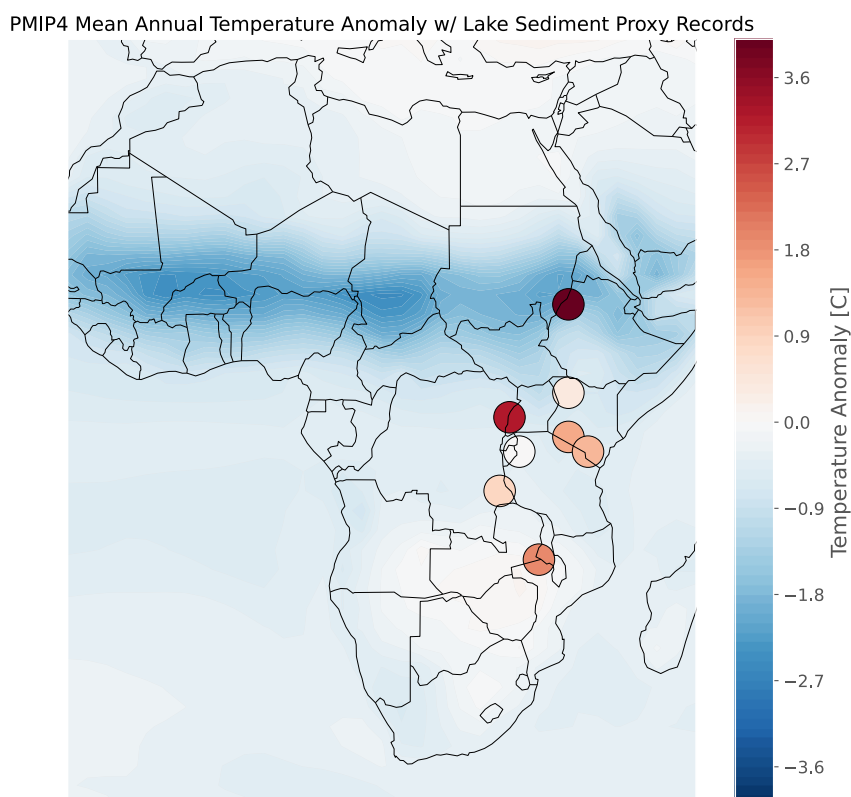


Figure 1. Map comparing Mid-Holocene temperature anomalies relative to Pre-Industrial for the PMIP4 multi-model ensemble mean (colored contours) and a suite of lake temperature reconstructions based on sediment GDGT proxy records (circles) for lakes Challa, Mahoma, Malawi, Rutundu, Tanganyika, Tana, Turkana, and Victoria (colored circles). See Table S1 in Supporting Information S1 for source of lake temperature records.

insolation resulted in increased boreal summer rainfall over northern Africa (deMenocal et al., 2000; Jousaume et al., 1999; Shanahan et al., 2015). This resulted in widespread vegetation throughout the Saharan region, suppressed atmospheric dust levels, enhanced water vapor, and decreased planetary albedo. Some studies have suggested that these responses also contributed to higher global temperatures (Thompson et al., 2022).

At present, multiple reconstructions of African hydroclimate are available spanning different time periods and regions (Tierney et al., 2008, 2011, 2015), which facilitate paleoclimate model-data comparison for model variables like precipitation (Chevalier et al., 2017). Similar, though more limited in number, efforts to build temperature reconstructions from tropical African lake sediments have yielded important records of past temperature change. However, recent paleoclimate data-model comparisons for Africa indicate significant data-model disagreement in the past. Geochemical proxy-based temperature reconstructions from lakes (Berke et al., 2012; Garelick et al., 2022; Powers et al., 2005; Tierney et al., 2008), pollen (Ivory & Russell, 2016), and glacier retreat evidence (Jackson et al., 2020) suggest regions of eastern tropical Africa were up to 2°C warmer than the historical period during the MH (Loomis et al., 2017; Powers et al., 2005; Tierney et al., 2008). Previous work showed that models from the Paleoclimate Modeling Intercomparison Project Phase 3 (PMIP3) fail to simulate this warming at Lakes Tanganyika and Malawi (Dee et al., 2021), and that most PMIP3 models simulate MH cooling. Furthermore, Brierley et al. (2020) show that PMIP Phase 4 (PMIP4) models simulate MH annual temperature anomalies that are cooler than PMIP3, both globally and in Africa. To summarize prior proxy and model results, Figure 1 compares a suite of temperature anomalies from sediment-based reconstructions in tropical East Africa (Table S1 in Supporting Information S1), all of which show warming in the MH with respect to the pre-Industrial (PI), to the ensemble mean of PMIP4 MH simulations, which show continent-wide cooling. Additional pollen-based reconstructions support the direction and magnitude of these sediment-based reconstructions (Bartlein et al., 2011). Figure S1 in Supporting Information S1 shows a comparison of these pollen records to the PMIP4 ensemble mean; although these records house large uncertainties, they indicate that

Table 1
Boundary Conditions Used in Each PMIP3 and PMIP4 Experiment for the Mid-Holocene and Pre-Industrial

	MH PMIP3	MH PMIP4	PI PMIP3	PI PMIP4
Eccentricity	0.018682	0.018682	0.016724	0.016724
Obliquity	24.105°	24.105°	23.446°	23.446°
Perihelion-180°	0.87°	0.87°	102.04°	100.33°
Vernal equinox	3/21 noon	3/21 noon	3/21 noon	3/21 noon
CO ₂	280 ppm	264.4 ppm	280 ppm	284.3 ppm
CH ₄	650 ppb	597 ppb	760 ppb	808.2 ppb
N ₂ O	270 ppb	262 ppb	270 ppb	273 ppb
Solar constant	1,365 W/m ²	1,360.747 W/m ²	1,365 W/m ²	1,360.747 W/m ²

significant proxy/model disagreement exists throughout Africa in the MH. This discrepancy, the so-called “Holocene temperature conundrum” (see e.g. Kaufman and Broadman (2023)), could indicate bias in climate model projections of future global temperatures (Z. Liu et al., 2014). Proxy uncertainties undoubtedly contribute to this proxy/model disagreement, especially as a result of seasonal biases (see e.g. Bova et al. (2021); Dee et al. (2021)), but it is unlikely that seasonal variations and bias alone are the dominant cause of proxy-model uncertainty near the equator; in the southern African tropics, temperatures do not vary more than ~2°C over the annual cycle. Proxy/model discrepancies may also result from the fact that proxies reconstruct lake temperature rather than air temperature, causing a partial temperature offset (Dee et al., 2021). On the other hand, many PMIP models do not accurately prescribe or simulate proxy-derived estimates of precipitation, dust, and vegetation cover during the MH, all of which impact temperature (Harrison et al., 2014). Broadly speaking, some combination of proxy error and model bias must account for the observed temperature disparity during the MH.

This work specifically investigates potential causes of the MH-PI model-proxy temperature disagreement arising from the *PMIP models alone*. In doing so, we provide guidance for changes needed to move toward more complete and interactive Earth System models (in terms of their boundary conditions, physics, parameterizations, and processes). We suggest future avenues for experiments that may further reduce paleoclimate data-model discrepancies. We focus on three key questions: (a) What drives inter-model spread in simulated African temperatures during the MH?; (b) What are the key differences between PMIP3 and PMIP4 in terms of the temperature response to boundary conditions?; and finally, (c) What processes and boundary conditions have the largest impact on simulated temperatures, and what does this imply for model physics choices? Section 2 describes the model simulations employed in this work and our analysis methodology. Section 3 evaluates the controls on African air temperature during the MH in multiple climate model experiments, and Section 4 discusses the implications of our results.

2. Methods

2.1. Model Simulations

We analyzed GCM simulations from PMIP3 and PMIP4 (Braconnot et al., 2012; Brierley et al., 2020; Kageyama et al., 2017; Meinshausen et al., 2011) with publicly-available output sufficient for a surface energy budget decomposition; the details of all of the model experiments employed in this analysis are given in Tables S2 and S3 in Supporting Information S1. Modeling groups participating in PMIP conducted experiments simulating the MH with prescribed orbital parameters, including large changes to precessional forcing compared to the modern, and greenhouse gas concentrations (Otto-Bliesner et al., 2017) (Table 1). We analyzed both PMIP3 and PMIP4 model ensembles, as PMIP4 used lower concentrations of greenhouse gas and a different solar constant for the MH compared to PMIP3, which allows us to investigate the relative impacts of the different forcings on GCM-simulated temperatures over Africa.

To further evaluate MH model simulation choices and their impacts on temperature, we analyzed two sets of sensitivity experiments that altered dust and vegetation boundary conditions. First, Braconnot et al. (2021) conducted three experiments with the IPSLCM6A-LR GCM (Boucher et al., 2020) using common PMIP4 MH

orbital and greenhouse gas boundary conditions, but each with different dust forcing. The *No Dust* experiment completely suppresses dust in the model run, while the *Albani0k* and *Albani6k* experiments use dust boundary conditions reconstructed from paleodust archives (Albani & Mahowald, 2019). We compare [No Dust]-[Reference IPSLCM6A-LR MH experiment] and [Albani6k-Albani0k] to constrain the impact of dust on African climate during the MH. All three experiments (*No Dust*, *Albani0k*, *Albani6k*) have reduced dust concentrations compared to the standard PMIP4 MH reference simulation. Additionally, *Albani6k* has reduced dust compared to *Albani0k*. Second, we evaluated a *Green Sahara* experiment conducted using the EC-EARTH GCM (Gaetani et al., 2017; Pausata et al., 2016), wherein standard PMIP3 MH boundary conditions were used but dust levels were reduced by up to 80% and the entire Sahara vegetation surface was set to evergreen shrub.

2.2. Analyses

We examine the drivers of model temperature to better understand the extent to which model uncertainties contribute to the MH temperature disagreement. To accomplish this, this study deconvolves the PMIP GCMs' surface energy budgets (SEB) following Izumi et al. (2015) and examines variables likely to control changes in temperature between the MH and PI, including shortwave and longwave radiation, cloud cover, precipitation, and latent and sensible heat. This technique applies the principles of energy balance and the Stefan-Boltzmann law to express temperature change in terms of shortwave and longwave radiation for both cloudy and clear-sky conditions, sensible and latent heat, as well as subsurface heat storage. The SEB decomposition partitions the overall surface temperature change to the individual energy fluxes at the surface-atmosphere interface. Each term, or energy flux, in the SEB decomposition is expressed in degrees Celsius, directly linking it to the overall surface temperature change. Thus, this method allows us to determine the primary drivers of surface temperature change in each model. Because this method is applied to *surface* energy budgets, temperature change is calculated in terms of skin temperature (the variable *TS* in PMIP models). A small residual term is produced, which is the difference between the model-simulated temperature difference and the temperature difference calculated as the sum of the SEB terms' temperature effects; the residual results from differences in models' emissivity constants. We calculated this decomposition for all grid points after output from each model was calendar corrected following Bartlein and Shafer (2019), re-gridded to a common $2^\circ \times 2^\circ$ grid, and a land mask was applied to avoid grid points over the ocean. We paid special attention to the southern tropics (-15 to $0N$, -15 to $50E$) to avoid averaging away competing seasonal differences north and south of the equator in the annual mean, and because this is the region with the most proxy temperature reconstructions using glycerol dialkyl glycerol tetraethers (GDGTs) (Figure 1) (Dee et al., 2021; Loomis et al., 2017; Tierney & Tingley, 2015). Although pollen-based temperature reconstructions do exist for the entire continent (see Figure S1 in Supporting Information S1), the GDGT records are more precise than pollen and directly record temperature. We computed the surface energy budget decomposition for all PMIP MH simulations and for the IPSL dust sensitivity tests; we were unable to complete the decomposition for the EC-EARTH Green Sahara experiments, however, because necessary variables for the decomposition were not saved.

To analyze potential causes of the temperature spread in PMIP simulations, we examined the upper and lower bounds of model temperature behavior by determining the warmest and coldest models for both PMIP3 and PMIP4 as defined by the MH-simulated near-surface temperature relative to the PI (i.e., the coldest model has the lowest average MH temperature relative to its PI simulation, and the warmest model has the highest average MH temperature relative to its PI simulation). For this analysis we used the near-surface air temperature variable (TAS) (the outcome is the same using skin temperature (TS)), taking the time-series and spatial average of near-surface temperature for the first 100 years after the end of the spin-up period over land in Africa between the equator and $15^\circ S$ to capture a tropical average. We then compared the PMIP model variables related to surface heat budgets: near-surface air temperature (TAS), downwelling shortwave radiation (RSDS), precipitation (PR), and cloud cover (CLT) in the warmest and coldest models to the multi-model ensemble mean.

3. Results

The differences between the multi-model average of PMIP4 simulations and PMIP3 simulations of the MH (Brierley et al. (2020), and see Figure S3 in Supporting Information S1) indicate that PMIP4 simulations are, on average, approximately $1^\circ C$ cooler over continental Africa than the PMIP3 simulations. PMIP4 boundary conditions include lower concentrations of CO_2 , methane, and nitrous oxide, so lower temperatures are expected due to lower longwave forcing (Table 1). PMIP3 models simulate an average of $0.95^\circ C$ of cooling in tropical Africa in

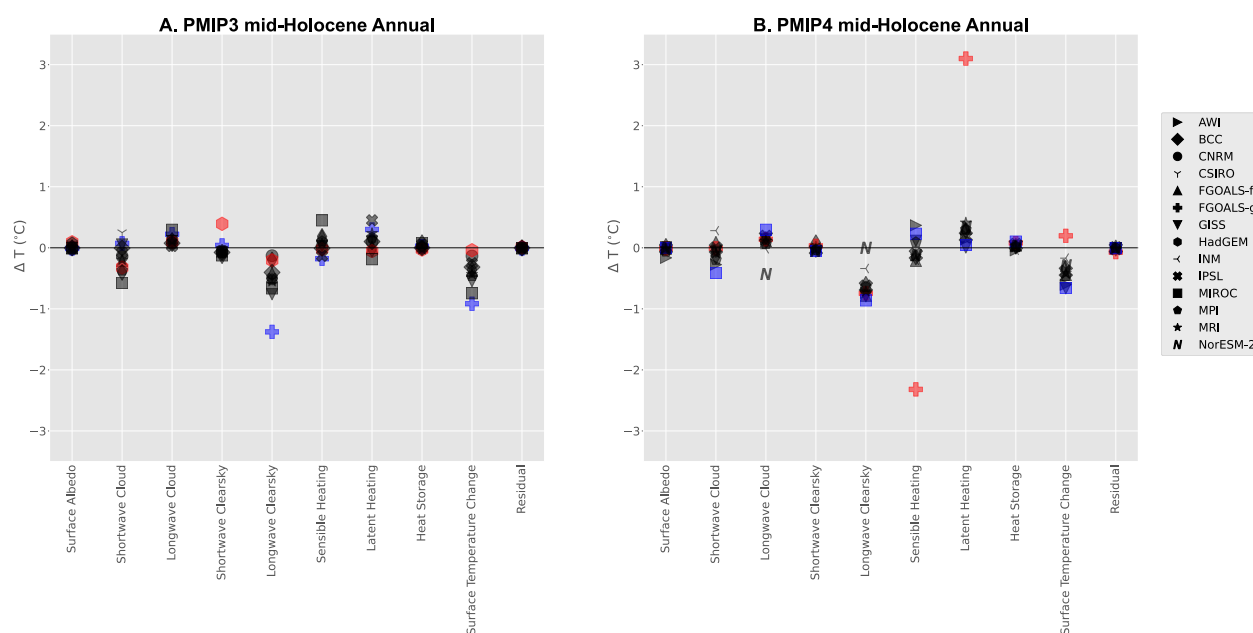


Figure 2. Surface energy budget decomposition for southern tropical Africa [(0, 15)S, (−15, 50)E] for PMIP3 (a) and PMIP4 (b) Mid-Holocene experiments expressed as temperature anomalies relative to the respective PI control simulation. Blue and red symbols represent the coldest and warmest model, defined as the model that is coldest or warmest relative to its PI control. The first eight columns each represent one energy flux variable in the decomposition and its impact on mean annual skin temperature. The eight energy flux terms sum to equal the surface temperature change plus the residual.

the MH compared to the PI, while PMIP4 models simulate an average 1.3°C of cooling compared to the PI experiments. Although the boundary conditions, specifically greenhouse gas forcing, may explain much of the temperature difference between PMIP3 and PMIP4 simulations of the MH, Figure S3 in Supporting Information S1 shows that the monsoon region is even cooler compared to the rest of the continent in PMIP4 relative to PMIP3.

We first evaluate temperature differences between PMIP3 and 4 using the surface energy budget decomposition method to diagnose the drivers of temperature changes in the PMIP ensemble during the MH (Section 3.1). We then evaluate the two sets of sensitivity experiments varying both dust and vegetation forcing (Section 3.2).

3.1. Surface Energy Budget (SEB) Decomposition

3.1.1. Annual SEB

Figure 2 shows the SEB decomposition (with the temperature impact of each term in degrees Celsius) for PMIP3 (A) and PMIP4 (B) for annual temperature anomalies relative to the PI for the southern tropics. The terms in Figure 2 from left to right capture the surface temperature effects of MH-PI changes in: surface albedo on surface absorbed shortwave radiation (e.g., from vegetation), cloud effects on surface downwelling shortwave radiation, cloud effects on surface downwelling longwave radiation, clear-sky effects on surface downwelling shortwave radiation (e.g., from changes in insolation or shortwave absorption by water vapor or carbon dioxide), clear-sky effects on surface downwelling longwave radiation, surface-air sensible heating, surface-air latent heating, and subsurface heat storage.

The SEB decomposition for both PMIP3 and PMIP4 simulations indicates that the largest contributions to MH cooling in the southern tropics come from changes in the longwave clearsky term. The longwave clearsky term combines several processes: (a) changes in atmospheric greenhouse gases (trace gases, water vapor), (b) the longwave-temperature feedback, wherein a change in surface temperature due to another SEB term alters the amount of longwave radiation emitted at the surface, amplifying the overall temperature change, and (c) changes in atmospheric heat transport. For (a), we expect that, given the known MH external forcings (Table 1), greenhouse gas (GHG) concentrations have a limited impact on MH cooling, but that water vapor feedbacks could play a role. For 2), it appears that the longwave-temperature feedback (e.g. Sejas & Cai, 2016 and their Figure 1)

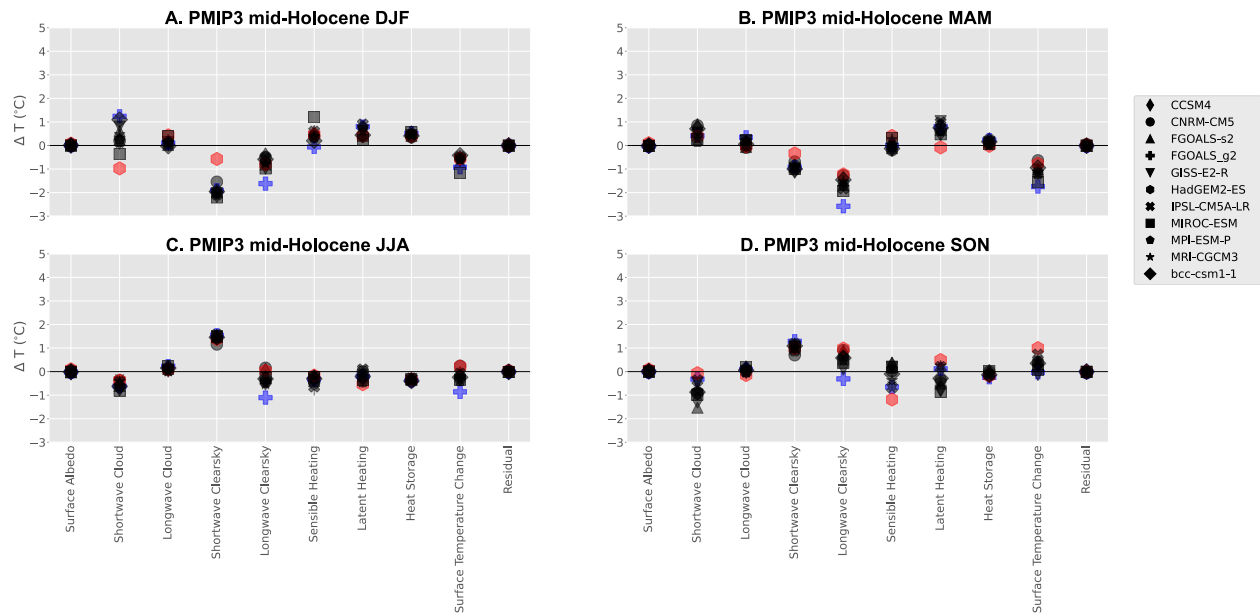


Figure 3. Seasonal surface energy budget decomposition for southern tropical Africa [(0, 15)S, (−15, 50)E] for PMIP3 Mid-Holocene experiments DJF (a), MAM (b), JJA (c), and SON (d). Blue and red symbols represent the coldest and warmest model, defined as the model that is coldest or warmest relative to its PI control. The first eight columns each represent one energy flux variable in the decomposition and its impact on mean seasonal skin temperature. The eight energy fluxes sum to equal the surface temperature change plus the residual.

amplifies cooling due to cloud forcing. Negative shortwave cloud values (Figure 2) indicate that cloudier conditions relative to the PI result in less shortwave radiation reaching the surface, contributing to cooling, even though this is somewhat counterbalanced by the warming effects of clouds via increased longwave. The sensible and latent heating terms capture the impacts of changing evapotranspiration on local temperatures; latent heat loss to evaporation is the dominant temperature flux from the ground to the air in moist environments, and sensible heat loss dominates in arid climates where evaporation does not occur. These terms are difficult to interpret in the annual mean, which averages over both wet and dry seasons, but show clearer patterns in seasonal analyses (discussed in Section 3.1.2). Lastly, (c) changes in heat *transport* (e.g., advection) are not calculated here, but other studies show that PMIP3 models exhibit changes in zonal heat transport (Donohoe et al., 2020; X. Liu et al., 2017; McGee et al., 2014), and an analysis of PMIP4 IPSL experiments showed reduced (increased) moist static energy transport across the southern African tropics during January–February (July–August) in the MH compared to the PI (see Braconnot et al. (2021) Figure 9, panel a and b). Other terms in the SEB decomposition, including surface albedo forcing, shortwave clear-sky forcing, and heat storage effects are generally close to zero, indicating negligible effects on temperature in the annual mean.

Although the models are generally tightly grouped in the SEB decomposition, FGOALS-g3, the PMIP4 model with the least MH cooling, has an anomalously high temperature response to changes in sensible and latent heat. These two variables are related and together indicate a more arid MH climate in this model: a positive value for the latent heating term indicates warming due to less energy lost to the latent heat of evaporation (essentially, less latent heat flux from the surface); a negative sensible heating term indicates more sensible heat flux because the land is drier (Sutton et al., 2007). FGOALS-g3 seems to simulate a larger change in aridity in the southern tropics region compared to other PMIP4 models, a signal that is also observed in other subtropical regions for this model (de Wet et al., 2023).

3.1.2. Seasonal SEB

The seasonal SEB decomposition for the southern tropics (Figures 3 and 4) shows large seasonal variations in temperature drivers during the MH compared to the PI: DJF/MAM show approximately 1°C of cooling, whereas JJA/SON show less cooling or slight warming. This partially follows from the fact that temperature changes during the MH were forced by large changes in seasonal insolation driven by precessional forcing. The shortwave

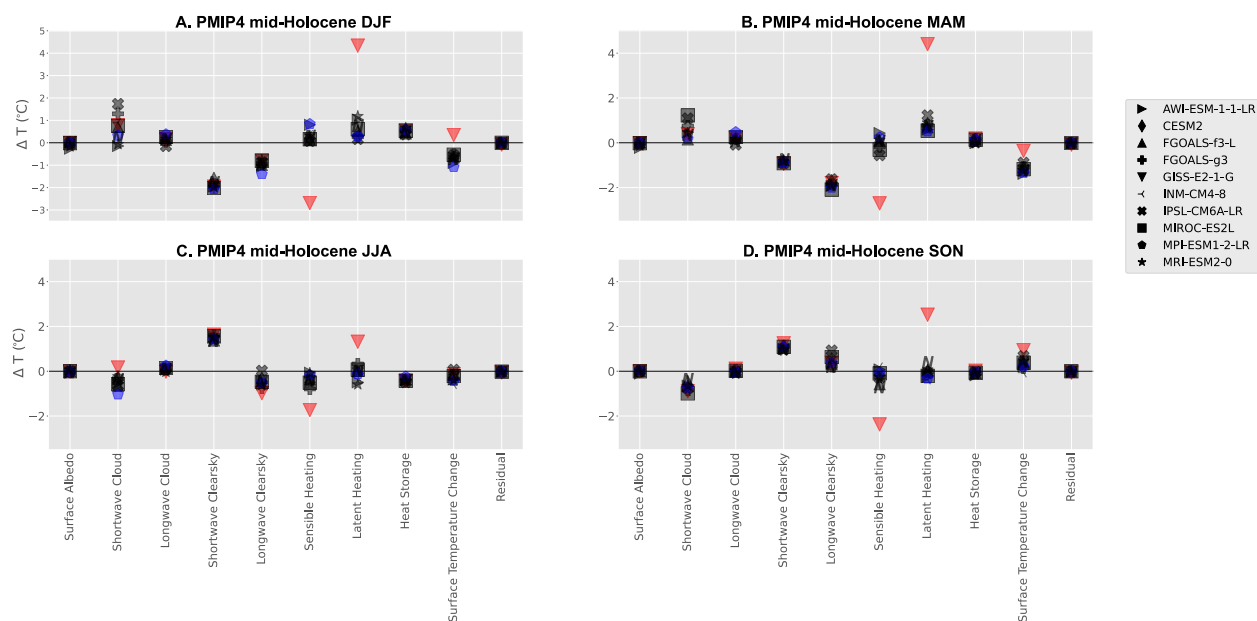


Figure 4. Seasonal surface energy budget decomposition for southern hemisphere tropical Africa [(0, 15)S, (−15, 50)E] for PMIP4 Mid-Holocene experiments DJF (a), MAM (b), JJA (c), and SON (d), as in Figure 3.

clearsky term, which captures insolation changes, emerges in the SEB decomposition as a key driver of seasonal temperature differences in the MH, showing a strong warming effect for JJA/SON (Figures 3 and 4 panels C and D) and a strong cooling effect for DJF/MAM (Figures 3 and 4 panels A and B). For all seasons except JJA, the longwave clearsky term appears to amplify the temperature effects of shortwave clearsky via the longwave temperature feedback, together acting as the primary drivers of temperature change. In JJA, increased insolation warms the surface via the shortwave clearsky term, but the longwave clearsky term provides a cooling effect in most of the PMIP3 and 4 models. While changes in moist static energy transport could be responsible for some cooling seen in the longwave clearsky term during JJA (Braconnot et al., 2021), there are also large decreases in MH water vapor in the southern tropics relative to PI in JJA that are not present in SON (Figure S2 in Supporting Information S1), indicating that water vapor feedbacks are contributing to the longwave clearsky term. These feedbacks appear key in determining the mean annual temperature by cooling surface temperature during a season in which warming would be expected due to orbital forcing.

The SEB decompositions shown thus far are only for the southern tropics, but we also examined the drivers of temperature for the whole continent. Figures 5 and 6 show maps of the multi-model ensemble mean for surface temperature, longwave clearsky, latent heating, and shortwave cloud for PMIP4. Results from PMIP3 are similar (not shown). While seasonal subtropical temperatures generally follow orbital forcing, the northern tropical monsoon region experiences cooling even in seasons where the rest of the continent is warming, driven by changes in the hydrologic cycle due to the strengthened monsoon. Although the monsoon region cools in every season, it is driven by changes in latent heating and shortwave cloud cover in JJA and SON, indicating cloudier conditions with more evaporation. In DJF and MAM the monsoon region cools as part of continent-wide cooling captured in the longwave clearsky term. To compare the seasonal SEB results to relevant seasonal proxy reconstructions, Figure S1 in Supporting Information S1 shows a comparison of the DJF and JJA PMIP4 ensemble mean MH surface temperature with pollen-based temperature reconstructions in the warmest and coldest month from Bartlein et al. (2011); like the GDGT reconstructions shown in Figure 1, there is disagreement between the JJA model temperatures and the proxy record in the monsoon region (on average, the pollen reconstructions indicate warmer JJA temperatures than PMIP4 models).

3.1.3. Interrogation of Relevant Hydroclimate Variables

Because the SEB decomposition indicates that variables related to the hydrological cycle are important in setting temperature, we analyze maps of three key model variables to evaluate their controls on near-surface air

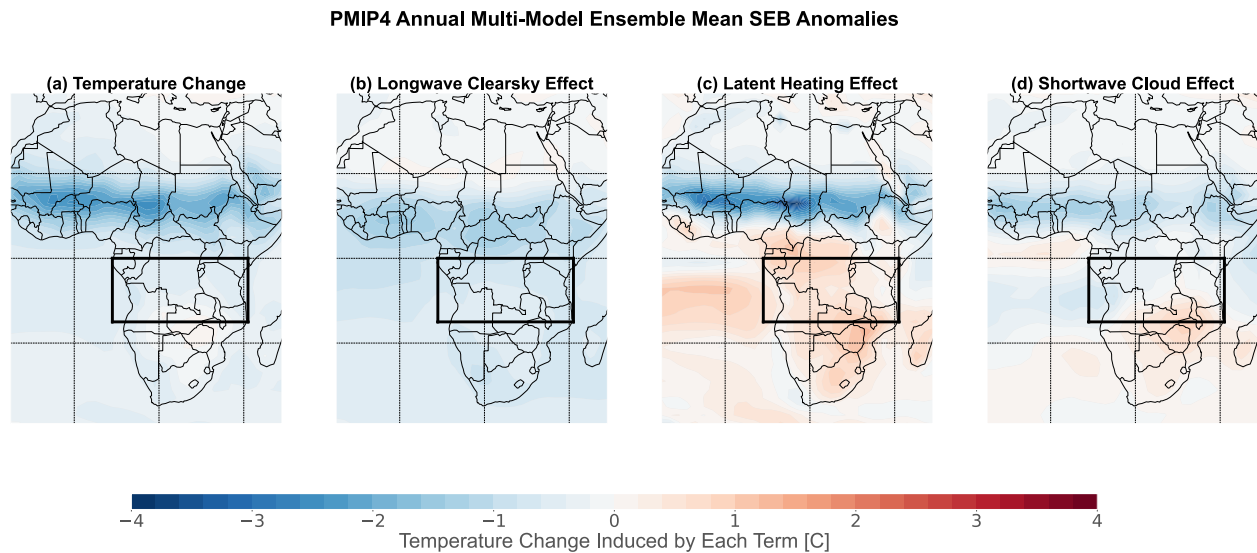


Figure 5. Maps showing spatial pattern for changes in the annual multi-model ensemble mean SEB decomposition terms skin temperature change (a), longwave clearsky effect (b), latent heating effect (c), and shortwave cloud effect (d). The boxes show the southern tropics region used for Figures 2–4. Anomalies are calculated relative to the PI. The maps b–d show the effect of each variable on the overall temperature change (a).

temperature: downwelling shortwave radiation, precipitation, and cloud cover. We analyzed two individual models each for PMIP3 and PMIP4 representing the coldest and warmest models for the MH in southern tropical Africa, and compared them to the multi-model ensemble mean to place upper and lower bounds on PMIP model temperature behavior. These variables were chosen because they are reasonably representative of hydrologic cycle feedbacks in response to temperature changes driven by shortwave forcing.

In PMIP3 simulations, we observe mean cooling during the MH compared to PI. Increased cloud cover and reduced downwelling shortwave radiation both contribute to colder temperatures during the MH (Figure 7), although the pattern is not spatially homogeneous; the signal is significant and especially pronounced over the Sahel. The PMIP4 simulations of the MH (Figure 8) in the ensemble mean similarly show continent-wide cooling that is significant and especially strong across the Sahel, corresponding to less downwelling shortwave radiation and more cloud cover regionally. Both PMIP3 and PMIP4 show consistent and significant changes in precipitation during the MH (Figures 7 and 8): enhanced precipitation accompanying increased cloud cover across the Sahel region, which jointly act to cool temperatures (Figure 8 panels G, H, I, J, K, and L). As shown in Figure 8, a large and significant reduction in shortwave radiation reaching the surface occurs in MIROC, the coldest model. The models that emerge as the coldest and warmest simulations are different between PMIP3 and PMIP4 generations. Although the spread between models is relatively small, the differences between warmest and coolest models closely mirror the differences in cloud cover and precipitation. This may suggest that the same processes (namely, hydroclimate changes) that drive cooling in the ensemble mean also determine the inter-model spread. Because SEB analysis (Figure 5) indicates that temperature feedbacks in response to changing hydroclimate drive MH cooling in PMIP simulations, the cooler monsoon region may explain some of the PMIP4-PMIP3 temperature differences that are not driven by GHG concentrations alone. Finally, to determine if the inter-model spread was caused by differences in the SEB terms, we plotted temperature change, longwave clearsky, shortwave cloud, and latent heat as a function of both (a) model resolution and (b) model equilibrium climate sensitivity, but no clear patterns emerged (not shown).

3.2. Adjusted Boundary Condition Experiments: Dust and Vegetation

To investigate uncertainties around the impacts of vegetation on continental-scale temperature change, and to assess how much of the mismatch between model simulations and proxy reconstructions may be driven by these uncertainties, we examine two additional sensitivity experiments, one using the PMIP3 EC-EARTH model and the other using the PMIP4 IPSL model, each of which changed boundary conditions related to the Green Sahara.

PMIP4 Seasonal Multi-Model Ensemble Mean SEB Anomalies

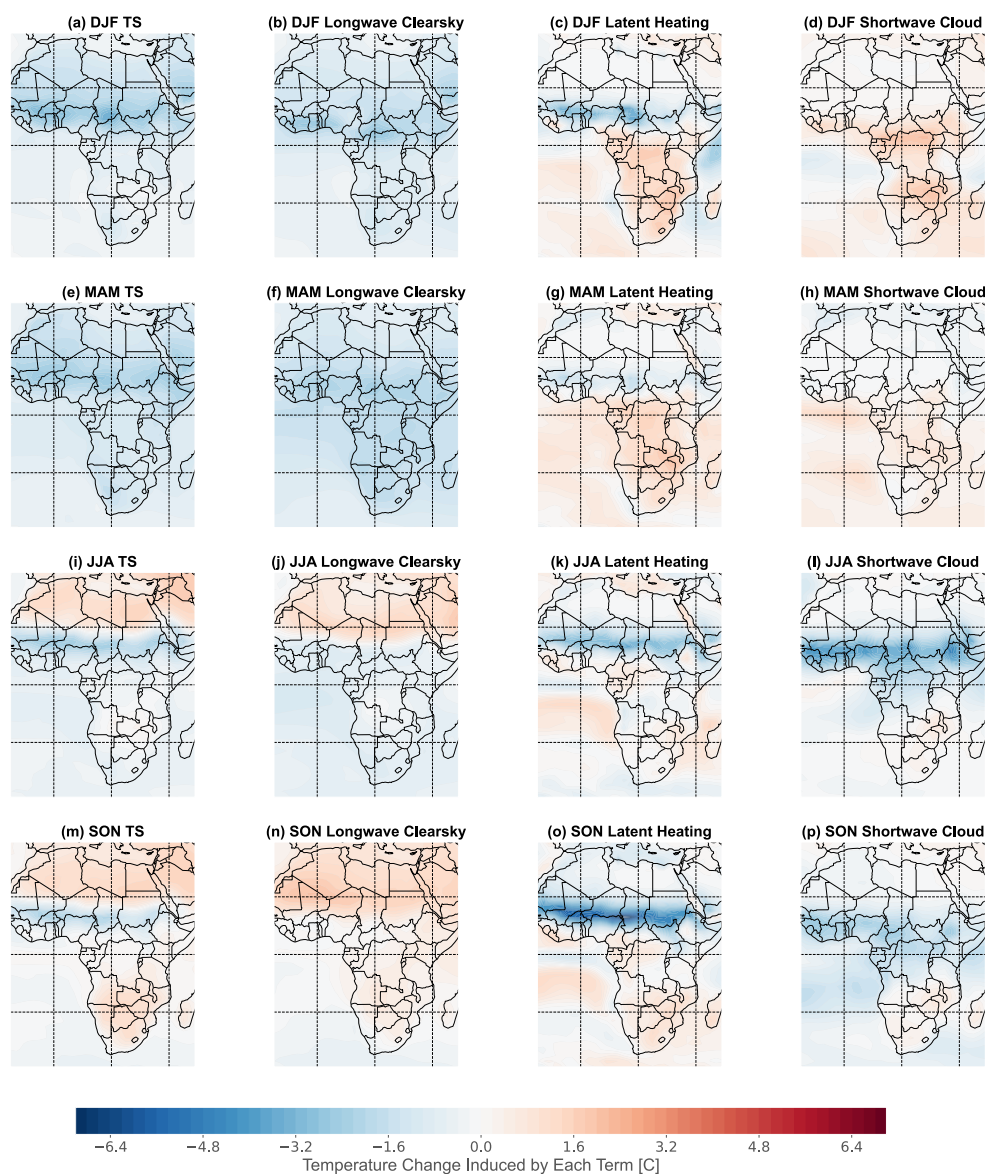


Figure 6. Maps showing the spatial pattern for changes in the seasonal multi-model ensemble mean SEB decomposition terms skin temperature change (a, e, i, m), longwave clearsky effect (b, f, j, n), latent heating effect (c, g, k, o), and shortwave cloud effect (d, h, l, p). Anomalies are calculated relative to the PI. The maps in the second, third, and fourth columns show the effect of each variable on the overall temperature change (first column).

3.2.1. Dust

A comparison between three IPSL experiments that altered dust aerosol forcing, described in Braconnot et al. (2021), is shown in Figure 9. Dust scatters incoming solar radiation and outgoing longwave radiation, which can result in competing temperature effects. Generally, however, the net impact of dust is to cause surface cooling (Kok et al., 2023; Y. Liu et al., 2018). Consequently, the *No Dust* experiment shows warmer temperatures compared to the standard IPSL PMIP4 MH simulation, particularly over northern Africa (Figure 9). The warming relative to the standard PMIP4 MH experiment is pronounced and statistically significant over the Sahel, where the reduced dust forcings contribute to as much as 1°C of temperature change (Figure 9). The *Albani6k* experiment shows slightly warmer temperatures compared to *Albani0k* over the Sahel, but the temperature change between the two *Albani* dust experiments is mostly not significant. The temperature change in the southern

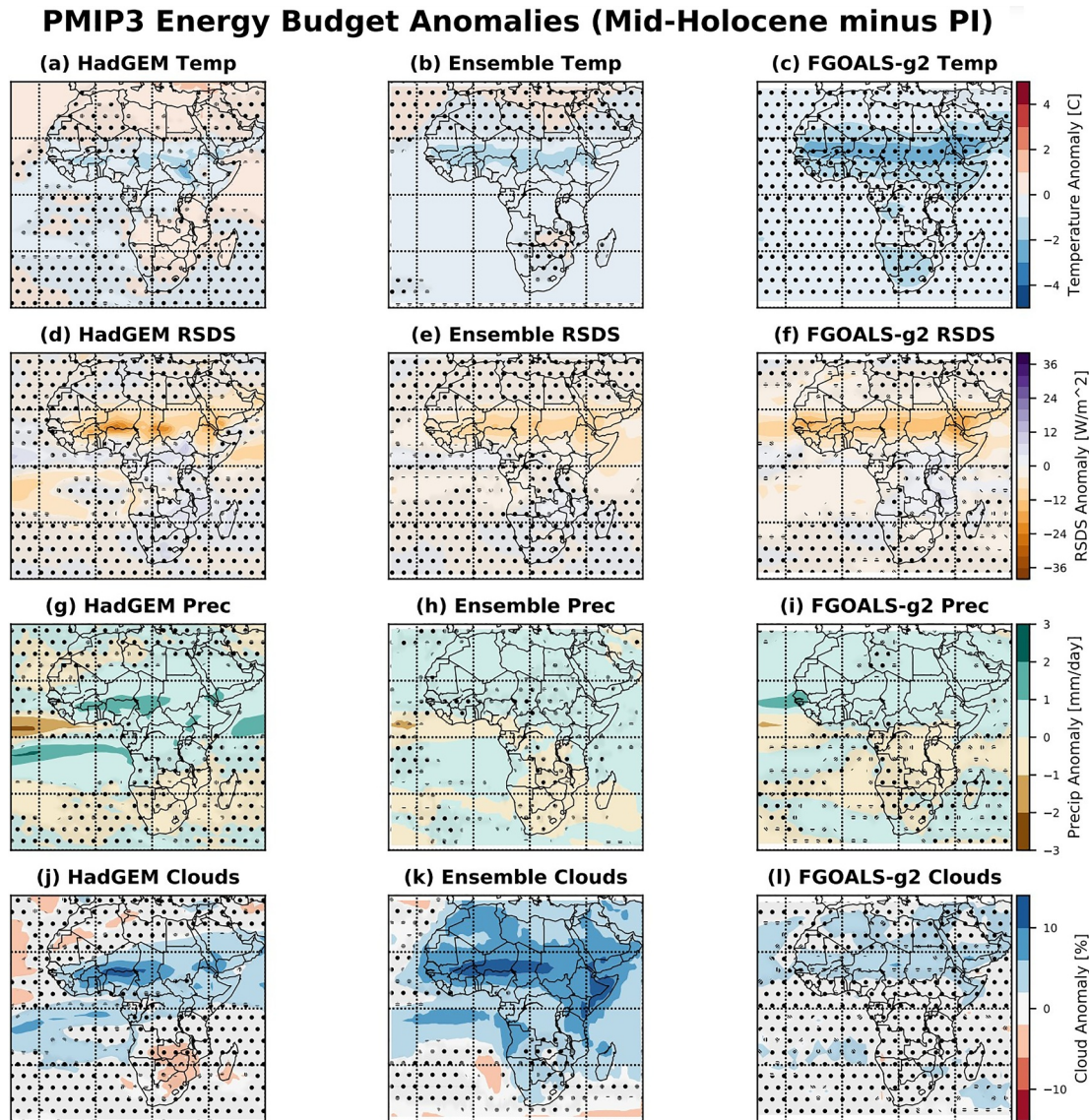


Figure 7. PMIP3 model anomalies (MH-PI), key variables impacting the energy budget for the warmest (HadGEM, a, d, g, j), ensemble mean (b, e, h, i), and coldest (FGOALS-g2, c, f, i, l) models during the MH. (a, b, c): temperature anomalies ($^{\circ}\text{C}$); (d, e, f): shortwave radiation anomalies (W/m^2); (g, h, i): precipitation (mm/day); (j, k, l): cloud fraction (%). Stippling represents differences that are not significant at the 95% level.

tropics, where many of the lake sediment proxy records are located, is 0.18°C for the *No Dust* simulation; while this is not enough to reconcile the proxy/model discrepancy, statistically significant surface warming does occur. The warming in the Sahel also more closely resembles pollen reconstructions from Bartlein et al. (2011) (and see Figure S1 in Supporting Information S1).

We also conducted the same surface energy balance decomposition for the IPSL dust experiments with results shown in Figure 10. The two sets of experiments show broad consistency across many of the surface energy budget terms, but differ sharply in the magnitude of change. The shortwave clearsky term captures the cooling effects of dust as it scatters incoming shortwave radiation. As shown in Figure 9, this has a small temperature impact of approximately 0.1°C when averaged over the southern tropics. *Even with reduced or even zero dust forcing, however, neither of these dust experiments simulate a MH warmer than the PI.* The sensitivity experiments do show warming due primarily to longwave clearsky forcing, but there is also cooling due to latent heat losses. The SEB decomposition (Figure 10) thus suggests limits to the temperature impacts of dust since increases in latent cooling offset warming caused by increased downwelling shortwave radiation.

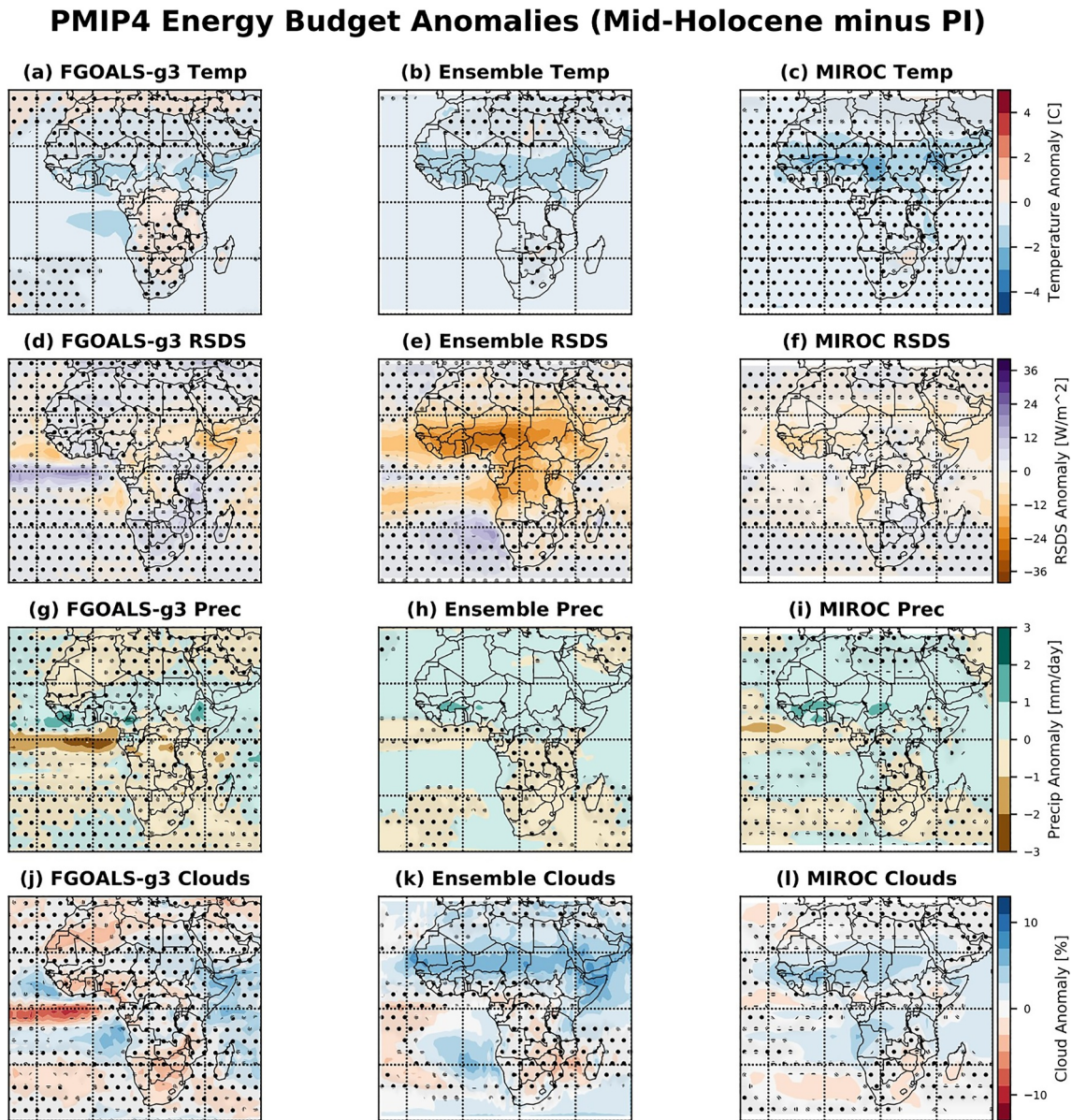


Figure 8. PMIP4 model anomalies (MH-PI), key variables impacting the energy budget for the warmest (FGOALS-g3, a, d, g, j), multi-model ensemble mean (b, e, h, i), and coldest (MIROC, c, f, i, l) models during the MH. (a, b, c): temperature anomalies ($^{\circ}\text{C}$); (d, e, f): shortwave radiation anomalies (W/m^2); (g, h, i): precipitation (mm/day); (j, k, l): cloud fraction (%). Stippling indicates differences are not significant at the 95% level.

3.2.2. Interactive Vegetation

Expanded vegetation across the Sahara in the MH could also impact temperature. Plants are darker than sand, meaning the surface albedo is reduced and causing the region to absorb more energy from the sun. Multiple models have thus employed either prescribed changes in vegetation or implemented interactive vegetation (e.g., O'ishi et al. (2021)), where the vegetation is computed by the model and coupled into an Ocean-Atmosphere-Vegetation (OAV) scheme. To investigate the potential role of the Green Sahara on model-simulated temperature, we first examined the difference between the average temperatures of the PMIP3 models that include an OAV scheme and those that do not (Figure 11, panel a, and see Chevalier et al. (2017) Table 3 for the list of which PMIP3 models include coupled vegetation). While models with coupled vegetation have been shown to expand the total vegetation over the Sahara relative to the PI (Hopcroft et al., 2017), the increase is still modest compared

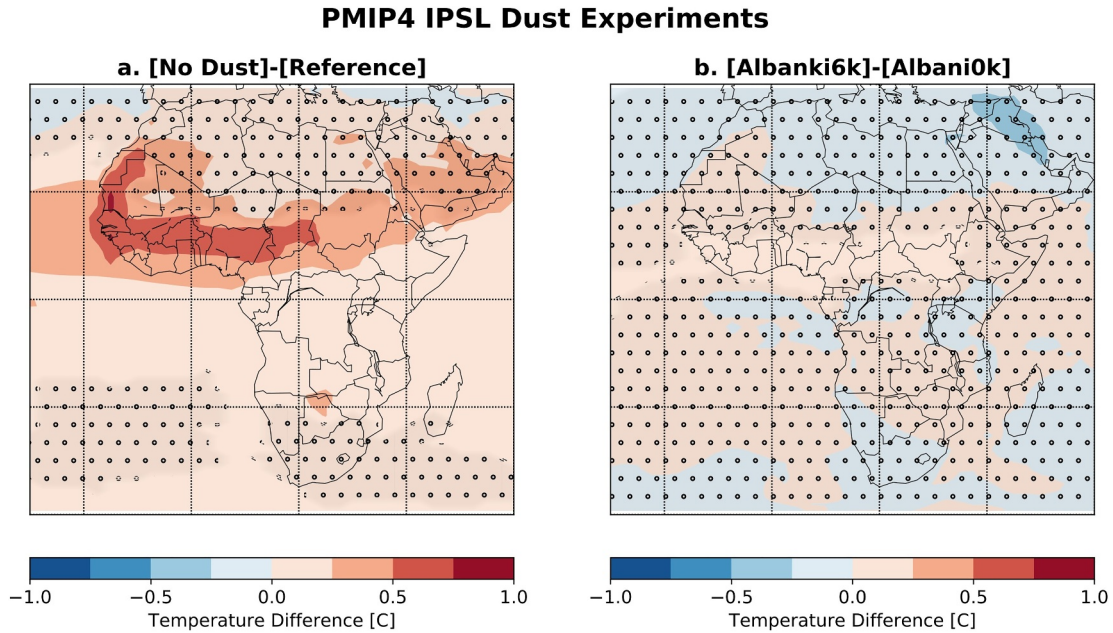


Figure 9. Impacts of different dust loadings on simulated temperature ($^{\circ}\text{C}$) in IPSL MH dust experiments. (a) *No Dust-Reference*, a comparison between a simulation with no dust and the standard PMIP4 mid-Holocene experiment (b) *Albani6k-Albani0k*, difference between two experiments using reconstructed dust levels for the mid-Holocene (6k) and pre-industrial period (0k) from Albani and Mahowald (2019). Stippling represents differences that are not significant at the 95% level.

to what paleovegetation reconstructions suggest during the MH (Renssen et al., 2006). The models with OAV do simulate a slight but statistically significant temperature increase compared to those with prescribed vegetation in some regions, especially at the northern and southern regions of the continent, but actually simulate cooler

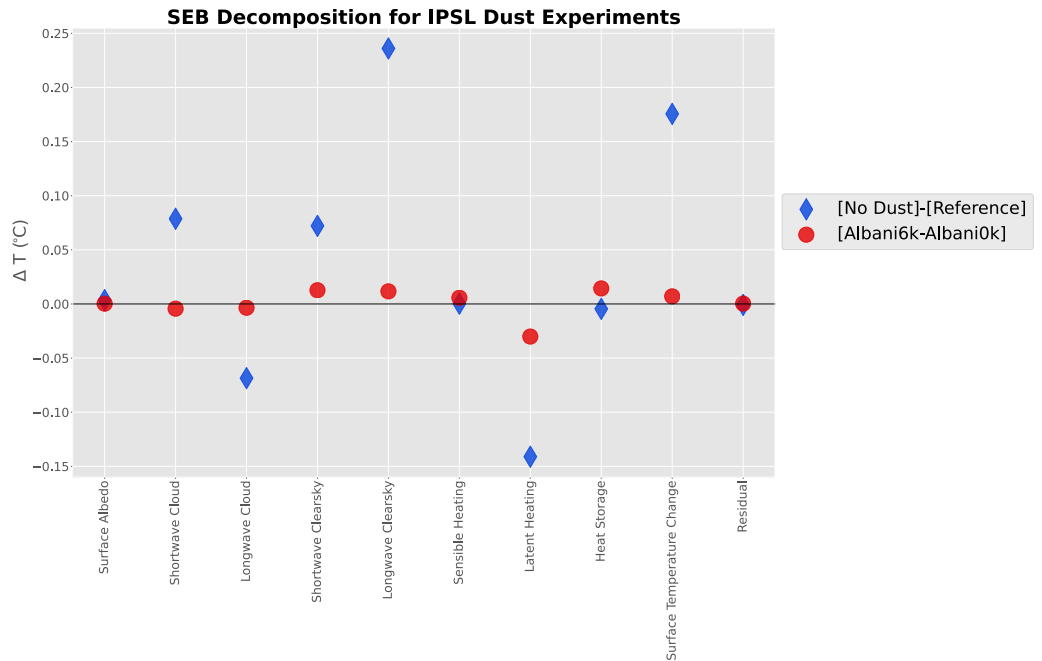


Figure 10. Surface energy budget decomposition for southern tropical Africa [(0, 15)S, (−15, 50)E] for IPSL MH dust experiments *No Dust-Reference* (a) and *Albani6k-Albani0k* (b). Each column represents the impact on mean annual near-surface air temperature that each variable has. Note that all experiments use MH orbital and greenhouse gas boundary conditions and vary only in their specification of dust.

Difference between PMIP3 Models with and without Interactive Vegetation

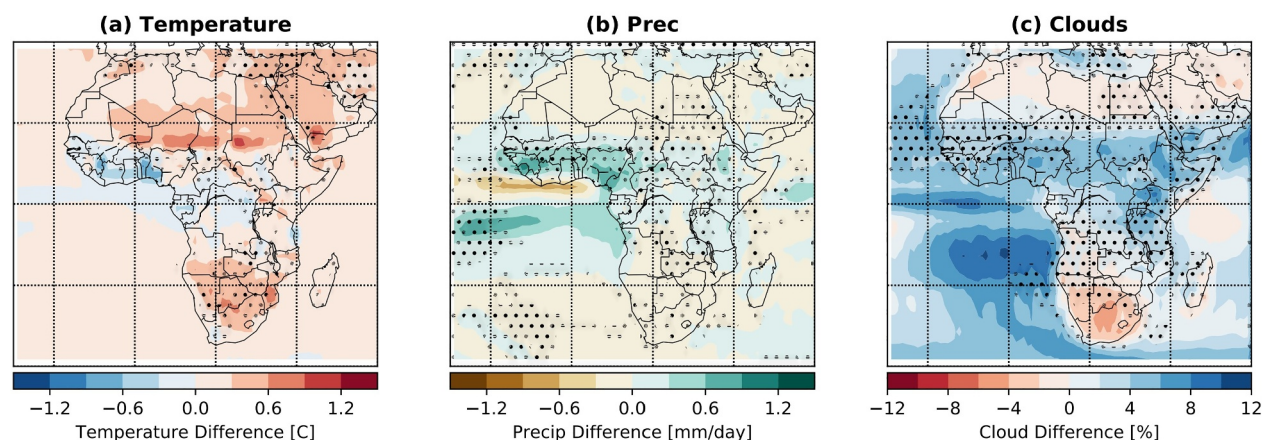


Figure 11. Difference between ensemble mean anomalies relative to the PI for annual temperature (a), precipitation (b), and cloud cover (c) for the MH simulations of all PMIP3 models with and all PMIP3 models without interactive vegetation (OAV schemes). Stippling represents differences that are not significant at the 95% level.

temperatures in the tropics (Figure 11). To investigate what caused this slight cooling, we also plotted the same prescribed/computed vegetation ensemble mean difference for precipitation and cloud cover (Figure 11 panels B and C). Areas where cooling takes place also feature more rain and cloud cover, indicating that the cooling response is potentially due to vegetation's impacts on the local hydroclimate, although these changes are not statistically significant except in the Saharan region. Note that Figure 11 shows the difference between two sets of MH experiments, not the temperature anomaly relative to the PI; the models with OAV still, on average, simulate MH cooling across the continent. Thus, the disagreement with available proxy records on the sign of temperature change remains.

Given that OAV scheme PMIP3 models does not correct the model-proxy temperature discrepancy, we evaluated two additional experiments with fully-prescribed extended vegetation over the Sahel and Sahara region (Gaetani et al., 2017; Pausata et al., 2016). These EC-Earth Model simulations make two key changes: (a) airborne dust levels are reduced by up to 80% (Figure 12a) and (b) the entire Sahara is prescribed as evergreen shrub (Figure 12b) (Gaetani et al., 2017; Pausata et al., 2016). These two changes in vegetation and dust concentrations lead to a remarkable warming over the Sahara, with an annual mean temperature peak of 9°C over northeastern Africa relative to the PI (Figure 12a). This Saharan warming more closely resembles the pollen reconstructions from Bartlein et al. (2011) (and see Figure S1 in Supporting Information S1). Moreover, the tropics ([-15 to 15N, -15 to 50E]) and southern Africa ([-30 to -20N, 15 to 30E]) show 1–2°C of warming relative to the control, and ~0.38°C of warming in the southern tropics. We also analyzed an experiment that prescribed vegetation changes without changing dust levels. Warming of up to 9°C is still present in the Sahara, but there is cooling relative to the PMIP3 EC-Earth MH experiment in tropical east Africa (Figure 12b). This cooling could be due to changes in rainfall distribution induced by changing dust levels (Pausata et al., 2016). The highly-variable temperature response to different land cover choices indicates accurate representations of land-surfaces may significantly improve model simulations of African climate.

4. Discussion: Simulating the Climate of the MH in Africa

This study seeks to understand the drivers of simulated temperatures during the MH in order to explore previously-reported paleoclimate proxy-model disagreement across this time horizon (Thompson et al., 2022), wherein proxy reconstructions show warmer temperatures during the MH but PMIP models simulate cooler temperatures. We analyzed key surface energy budget variables including precipitation, solar radiation and cloud cover and the relationship of these variables with temperature. Broadly speaking, our results show that all of the currently-available PMIP models simulate continent-wide annual mean cooling during the MH compared to the PI. This cooling is strongest in the Sahel, but also causes significant model-data mismatch in the southern tropics. Evaluation of the PMIP4 MH multi-model ensemble experiments analyzed by Brierley et al. (2020) show that,

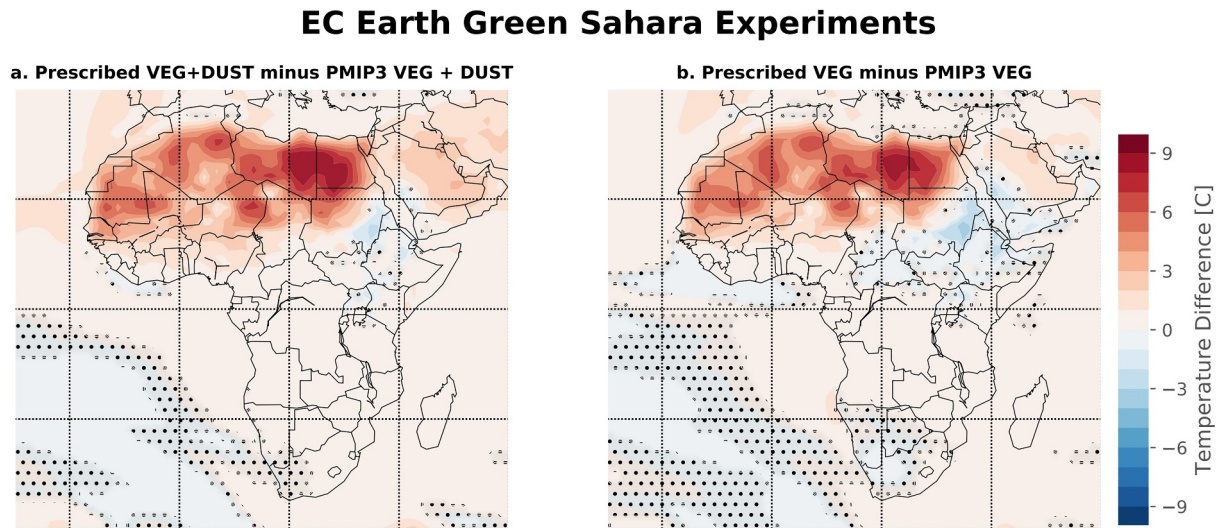


Figure 12. Impacts of Green Sahara Vegetation and Dust levels (a) and Green Sahara Vegetation only (b) on the mean annual simulated temperature for EC-Earth PMIP3 experiment. Stippling represents differences that are not significant at the 95% level.

although PMIP3 and PMIP4 simulate similar MH temperature anomalies in the southern tropics (Figure 2), multi-model average MH temperature anomalies for the Sahel are $\sim 1\text{--}2^\circ\text{C}$ colder for PMIP4 than PMIP3 (Figure S3 in Supporting Information S1). This is at least in part because PMIP4 employs lower (and more realistic) greenhouse gas concentrations compared to PMIP3. Unfortunately, the continent-wide cooling in PMIP4 simulations (relative to PMIP3 simulations) exacerbate previously-reported model-data disagreement during the MH (Section 1), as proxy records indicate warmer-than-PI temperatures during the MH (1 and see Figure S1 in Supporting Information S1 and Powers et al. (2005); Tierney et al. (2008); Berke et al. (2012); Garelick et al. (2022); Ivory and Russell (2016); Jackson et al. (2020); Bartlein et al. (2011)). Thus, we center our discussion here on the question: *what processes, if any, have a warming effect during the MH relative to PI?*

Our SEB analysis permits examination of the influence of each energy budget term on simulated temperature. Figures 2–4 indicate that amongst the standard PMIP3 and PMIP4 models, there is a consistent temperature response amongst models in terms of both the sign and amplitude of temperature change (albeit with small differences in SEB terms). MH cooling in PMIP3 and PMIP4 simulations is largely related to changes in the hydrological cycle. It is well established that both PMIP generations simulate a strengthened West African Monsoon (WAM) (Brierley et al., 2020), which is consistent with the sign (but not necessarily the amplitude) of change in proxy precipitation records (Williams et al., 2020). Maps of the SEB decomposition ensemble means (Figures 5 and 6) show that the strengthened monsoon drives cooling in the Sahel of up to 3°C . For the MH, increased cloudiness reduces downwelling shortwave and increased evaporation cools the surface. Longwave radiation in clear sky conditions plays an important role in generating and amplifying these cooling effects that PMIP models simulate during the MH, via forcing from greenhouse gases (e.g., CO_2 , water vapor) and the longwave-temperature feedback (Izumi et al., 2015). In the southern tropics, the SEB decomposition shown in Figures 3 and 4, additionally show an amplification of the seasonal cycle of shortwave clearsky forcing that translates to enhanced surface cooling during DJF and MAM, enhanced warming during SON, but unexpected cooling during JJA likely associated with water vapor feedbacks.

The spatial patterns of PMIP3 and PMIP4 temperatures in the warmest and coldest models (as defined by surface air temperature anomalies relative to the PI, Figures 7 and 8) suggest model spread in continent-wide cooling during the MH is driven in large part by the same hydrological cycle feedbacks at play in the ensemble mean, including changes in precipitation, cloud cover, and the resulting reduction in shortwave radiation reaching the surface (especially in the Sahel region). This response is consistent with SEB analyses, which show that changes in local hydroclimate are strong drivers of simulated MH cooling. This raises important questions surrounding the simulated temperature impact of a strengthened monsoon, and the potential for an exaggerated cooling response in PMIP models. Clouds play a crucial role in determining the temperature response to changing monsoon

intensity. PMIP models, however, may overestimate the cooling impact of clouds associated with the WAM. Previous work shows that CMIP models overestimate the strength of the low-cloud feedback in the tropics due to biases in optical cloud thickness (Nam et al., 2012) and cloud properties related to the WAM; these biases lead to overestimates in the longevity (Kniffka et al., 2019) and extent (Stein et al., 2015) of low-level cloud cover, both of which could lead to cooling.

All PMIP models simulate cooling during the MH compared to the PI across Africa in the annual mean, and in all seasons for the Sahel. Not only is the cooling response similar in magnitude across models, but there is little model spread in SEB terms. We posit that, assuming that the proxy reconstructions are unbiased, this consistent cooling response suggests a common source of temperature bias in models. Past work has shown that model treatment of vegetation and aerosols can drive differences between model simulations (Y. Liu et al., 2018); in agreement with this work, we found that while dust and vegetation, both separately (in the case of the IPSL experiment, Figure 9) and together (in the case of the EC-Earth experiment, Figure 12), do not resolve the proxy/model temperature difference, they do reduce the discrepancy. This could indicate that the greening of the Sahara, combined with additional feedback processes related to the West African Monsoon that are poorly represented in PMIP models, may be important in resolving the Holocene temperature conundrum.

There are three potential sources of model temperature bias during the MH explored in this work: dust, vegetation, and cloud feedbacks. We discuss the impacts of each individually:

1. *Vegetation*: Inaccurate representations of the Green Sahara could cause model-simulated cooling in the MH. Land-use/land-cover changes are a key boundary condition in other paleoclimate simulations (e.g., CESM-LME, Otto-Bliesner et al. (2015)), and prescribed vegetation, as shown in Section 3.3.2., can significantly warm the African continent. Although the temperature difference between PMIP3 models with and without interactive vegetation is very small (Figure 11 panel a), the EC-Earth experiment, which prescribed vegetation in the Sahara, showed significant warming (Figure 12). The heating driven by a vegetated Sahara comes from changes in surface albedo (Pausata et al., 2016). There are also effects on non-local climates, primarily due to expansion of the monsoon via the vegetation-precipitation feedback (Gaetani et al., 2017).
2. *Dust*: Dust in the atmosphere scatters incoming solar radiation, cooling the surface. As shown in Figure 10, dust forcing alters simulated MH temperature: reduced dust loads lead to surface warming via changes in shortwave clearsky forcing. Reducing dust leads to warming in both IPSL and EC-Earth experiments. However, dust particles have been shown in some cases to warm the atmosphere by absorbing longwave radiation (Chen et al., 2021), and the overall temperature effect of dust depends on its optical properties (Di Biagio et al., 2020). Previous works suggests that some dust particle sizes in Green Sahara experiments would have a limited climate impact (Hopcroft & Valdes, 2019), but Thompson et al. (2022) and Pausata et al. (2016), which have more absorbing dust in their models, show that dust reduction plays an important role in increasing the intensity of the West African Monsoon when the Sahara is vegetated. The Green Sahara experiment analyzed in our study is from Pausata et al. (2016), which uses a moderately absorbing dust and a scattering albedo of 0.89, which is low, but realistic for the iron-rich dust of the Sahara (Di Biagio et al., 2019).
3. *Clouds*: Boundary condition uncertainties for the Green Sahara also likely compound uncertainties in the temperature impact of a strengthened WAM. An intensified WAM results in expanded cloud cover over the Sahel region, further cooling surface temperatures. Dust affects the cooling impact of cloud cover: dust leads to longer lasting monsoon season cloud cover (via cloud nucleation) and alters the optical properties of the clouds, making them optically thicker and more reflective (Thompson et al., 2019). Therefore, reduced dust loads would offset the total cooling effect of a combined monsoon and dust surface temperature change (resulting in warmer conditions). PMIP models that correctly simulate a stronger monsoon may overestimate the cooling impact of this change, partially due to inaccurate representation of monsoon clouds, and partially due to inaccurate boundary conditions - namely, dust - related to the Green Sahara.

Of course, it is difficult to explain regional model behavior (e.g., temperature change in response to changes in the monsoon) without thorough examination of each model's code, parameter optimization experiments, or the ability to run simulations altering boundary conditions. Here, we investigated experiments with prescribed Green Sahara dust and vegetation changes. Other boundary conditions, such as realistic surface water (e.g., lakes) during the

MH, may also be required. Although both sets of sensitivity experiments we analyzed (dust in IPSL and EC-Earth, and vegetation in EC-Earth) induce some (approximately 0.5°C) MH warming over tropical land surfaces in Africa, different dust and vegetation levels may also trigger other temperature feedback mechanisms that further confound interpretation, or which are incompletely represented in models. We also note that this study has only analyzed one model with different vegetation cover (EC-Earth), and one additional model with altered dust (IPSL). Although these experiments do increase simulated surface temperatures in EC-Earth and IPSL, it is not necessarily true that other PMIP models would simulate the same increased temperatures or feedbacks, even if their vegetation and dust boundary conditions were changed in the same way. Targeted MH intercomparison simulations with identical dust and prescribed vegetation would be needed to confirm this.

It is also worth briefly discussing the relationship between temperature and precipitation on paleoclimate timescales. A comparison of tree, speleothem, and sedimentary records of the Asian monsoon, indicates that temperature and precipitation are *positively correlated* on long timescales (Rehfeld & Laepple, 2016). The PMIP3 models generally agree qualitatively with hydroclimate proxies for tropical East Africa in the MH (Chevalier et al., 2017): both show wetter conditions. It is possible that models correctly simulate moisture supply changes in the MH, while simultaneously cooling the surface *too much* in response to increased precipitation and cloud cover.

While improving the realism of our model boundary conditions is important, a critical need exists for clear frameworks to further test and update model physics. Some models reproduce a tipping point into a Green Sahara with simple known external forcings (Dallmeyer et al., 2021; Hopcroft et al., 2021), but others do not. During the transition from the last glacial maximum to the Holocene, precessional forcing drives higher insolation and precipitation, which should enhance vegetation and associated feedbacks. Yet multiple analyses of PMIP models outfitted with interactive vegetation indicates a notable shortcoming in most models to simulate this tipping point (Figure 11 and see e.g. Claussen et al. (2017)). Monsoon rain bands do not extend far enough to the north, limiting the expansion of vegetation. Even if we are confident that models' response to short- and long-wave forcing are correct, representations of atmosphere-vegetation feedbacks is likely still insufficient to simulate the Green Sahara and its associated climatic impact. Some sources of model uncertainty or bias, like vegetation extent (Thompson et al., 2022) or parameters related to atmospheric convection and dynamic vegetation (Hopcroft & Valdes, 2021), could be directly reduced via a combination of model simulations testing different parameterizations, further development of proxy records and quantification of their uncertainty, and analyses such as the SEB decomposition. Still other challenges related to atmospheric parameters (Ramos et al., 2022; J. Zhu et al., 2017), cloud water content (Zelinka et al., 2020), and mountain geometry (Baldwin et al., 2021) likely all compound uncertainties in model physics precluding accurate temperature simulations and are not addressed here.

In forthcoming work, we plan to investigate the model/proxy temperature discrepancy more explicitly with a set of temperature reconstructions from Africa. We will use output from the same suite of PMIP models analyzed in this study to force a proxy system model (PSM) for lake temperature (Dee et al., 2018) to facilitate a direct comparison to proxy-based temperature reconstructions. Extending the work of Dee et al. (2021), we will investigate sources of error in the proxy system itself, using the PSM to determine how much of the temperature difference may be due to proxy errors alone across the network of available proxy data spanning the full African continent. Future work could also explore connections between East Africa, a region of high proxy reconstruction density, and the Sahel/West African Monsoon region via the Walker Circulation (Funk et al., 2016).

5. Conclusions

Current-generation climate models project future temperature increases on the order of 5°C for the African continent. While regionally heterogeneous, the impacts of such severe temperature forcing on water availability, agriculture, and human health are likely to compound and worsen risks for African nations throughout the 21st century. Uncertainties in forcing and model physics jointly contribute to the relatively wide range of future temperature realities. Limitations surrounding model projections are critical to resolve to enable robust constraints on future African temperature change, effective mitigation and adaptation plans. To this end, this study evaluates available climate model simulations of the MH, an out-of-sample climate mean state target, to compare model performance. In particular, this study contributes to a better understanding of the “mid-Holocene conundrum,” (Z. Liu et al., 2014), indicating that part of the proxy-model temperature discrepancy may be due to

unrealistic model boundary conditions related to the Green Sahara, potentially amplified by feedbacks related to the WAM. Because these same models are used to project future climate change, refining projections requires a better understanding of what causes these discrepancies. Our results could indicate that model treatment of land type and aerosol loading are vitally important for model predictions of future temperature change in tropical Africa, meaning projections of features such as land use and deforestation are necessary to create robust predictions of climate change. Such information is needed to estimate risk, facilitate mitigation strategies for extreme heat and drought conditions, and accurately assess national security in developing African nations in a warming 21st century.

Data Availability Statement

CMIP5/PMIP3 and CMIP6/PMIP4 simulations used for this study (see Tables S2 and S3 in Supporting Information S1) are publicly available via <https://esgf-node.llnl.gov/>. GDGT lake surface temperature records for Figure 1 (see Table S1 in Supporting Information S1) are available from (Berke et al., 2012; Garelick et al., 2022; Loomis et al., 2015; Morrissey et al., 2017; Powers et al., 2005; Sinninghe Damsté et al., 2012; Tierney et al., 2008).

Acknowledgments

This work was supported by The National Science Foundation (NSF P2C2) Grants EAR-1903347 to S.D., EAR-1903345 to C.M., EAR-1903348 to J.M.R. We are grateful for the feedback of two anonymous reviewers which strongly improved this manuscript.

References

- Albani, S., & Mahowald, N. (2019). Paleodust insights into dust impacts on climate. *Journal of Climate*, 32(22), 7897–7913. <https://doi.org/10.1175/JCLI-D-18-0742.1>
- Baldwin, J. W., Atwood, A. R., Vecchi, G. A., & Battisti, D. S. (2021). Outsize influence of Central American orography on global climate. *AGU Advances*, 2(2), e2020AV000343. <https://doi.org/10.1029/2020AV000343>
- Bartlein, P. J., Harrison, S., Brewer, S., Connor, S., Davis, B., Gajewski, K., et al. (2011). Pollen-based continental climate reconstructions at 6 and 21 ka: A global synthesis. *Climate Dynamics*, 37(3–4), 775–802. <https://doi.org/10.1007/s00382-010-0904-1>
- Bartlein, P. J., & Shafer, S. L. (2019). Paleo calendar-effect adjustments in time-slice and transient climate-model simulations (paleocaladjust v1.0): Impact and strategies for data analysis. *Geoscientific Model Development*, 12(9), 3889–3913. <https://doi.org/10.5194/gmd-12-3889-2019>
- Berke, M. A., Johnson, T. C., Werne, J. P., Schouten, S., & Damste, J. S. S. (2012). A mid-Holocene thermal maximum at the end of the African humid period. *Earth and Planetary Science Letters*, 351, 95–104. <https://doi.org/10.1016/j.epsl.2012.07.008>
- Boucher, O., Servonnat, J., Albright, A. L., Aumont, O., Balkanski, Y., Bastrikov, V., et al. (2020). Presentation and evaluation of the IPSL-CM6A-LR climate model. *Journal of Advances in Modeling Earth Systems*, 12(7), e2019MS002010. <https://doi.org/10.1029/2019ms002010>
- Bova, S., Rosenthal, Y., Liu, Z., Godad, S. P., & Yan, M. (2021). Seasonal origin of the thermal maxima at the Holocene and the last interglacial. *Nature*, 589(7843), 548–553. <https://doi.org/10.1038/s41586-020-03155-x>
- Braconnot, P., Albani, S., Balkanski, Y., Cozic, A., Kageyama, M., Sima, A., et al. (2021). Impact of dust in PMIP-CMIP6 mid-Holocene simulations with the IPSL model. *Climate of the Past*, 17(3), 1091–1117. <https://doi.org/10.5194/cp-17-1091-2021>
- Braconnot, P., Harrison, S. P., Kageyama, M., Bartlein, P. J., Masson-Delmotte, V., Abe-Ouchi, A., et al. (2012). Evaluation of climate models using palaeoclimatic data. *Nature Climate Change*, 2(6), 417–424. <https://doi.org/10.1038/nclimate1456>
- Brierley, C. M., Zhao, A., Harrison, S. P., Braconnot, P., Williams, C. J. R., Thornalley, D. J. R., et al. (2020). Large-scale features and evaluation of the PMIP4-CMIP6 midHolocene simulations. *Climate of the Past*, 16(5), 1847–1872. <https://doi.org/10.5194/cp-16-1847-2020>
- Chen, S.-L., Chang, S.-W., Chen, Y.-J., & Chen, H.-L. (2021). Possible warming effect of fine particulate matter in the atmosphere. *Communications Earth & Environment*, 2(1), 208. <https://doi.org/10.1038/s43247-021-00278-5>
- Chevalier, M., Brewer, S., & Chase, B. M. (2017). Qualitative assessment of PMIP3 rainfall simulations across the eastern African monsoon domains during the mid-Holocene and the last glacial maximum. *Quaternary Science Reviews*, 156, 107–120. <https://doi.org/10.1016/j.quascirev.2016.11.028>
- Claussen, M., Dallmeyer, A., & Bader, J. (2017). *Theory and modeling of the African humid period and the green Sahara*. Oxford University Press. <https://doi.org/10.1093/acrefore/9780190228620.013.532>
- Dallmeyer, A., Claussen, M., Lorenz, S. J., Sigl, M., Toohay, M., & Herzschuh, U. (2021). Holocene vegetation transitions and their climatic drivers in MPI-ESM1.2. *Climate of the Past*, 17(6), 2481–2513. <https://doi.org/10.5194/cp-17-2481-2021>
- Dee, S. G., Morrill, C., Kim, S. H., & Russell, J. M. (2021). Hot air, hot lakes, or both? Exploring mid-Holocene African temperatures using proxy system modeling. *Journal of Geophysical Research: Atmospheres*, 126(10), e2020JD033269. <https://doi.org/10.1029/2020jd033269>
- Dee, S. G., Russell, J. M., Morrill, C., Chen, Z., & Neary, A. (2018). Prysm v2. 0: A proxy system model for lacustrine archives. *Paleoceanography and Paleoclimatology*, 33(11), 1250–1269. <https://doi.org/10.1029/2018pa003413>
- de Menocal, P., Ortiz, J., Guilderson, T., Adkins, J., Sarnthein, M., Baker, L., & Yarusinsky, M. (2000). Abrupt onset and termination of the African humid period: Rapid climate responses to gradual insolation forcing. *Quaternary Science Reviews*, 19(1), 347–361. [https://doi.org/10.1016/S0277-3791\(99\)00081-5](https://doi.org/10.1016/S0277-3791(99)00081-5)
- Detges, A. (2016). Local conditions of drought-related violence in sub-Saharan Africa: The role of road and water infrastructures. *Journal of Peace Research*, 53(5), 696–710. <https://doi.org/10.1177/0022343316651922>
- de Wet, C., Ibarra, D., Belanger, B., & Oster, J. (2023). North American hydroclimate during past warm states: A proxy compilation-model comparison for the last interglacial and the mid-Holocene. *Paleoceanography and Paleoclimatology*, 38(6), e2022PA004528. <https://doi.org/10.1029/2022PA004528>
- Di Biagio, C., Balkanski, Y., Albani, S., Boucher, O., & Formenti, P. (2020). Direct radiative effect by mineral dust aerosols constrained by new microphysical and spectral optical data. *Geophysical Research Letters*, 47(2), e2019GL086186. <https://doi.org/10.1029/2019GL086186>
- Di Biagio, C., Formenti, P., Balkanski, Y., Caponi, L., Cazaunau, M., Pangui, E., et al. (2019). Complex refractive indices and single-scattering albedo of global dust aerosols in the shortwave spectrum and relationship to size and iron content. *Atmospheric Chemistry and Physics*, 19(24), 15503–15531. <https://doi.org/10.5194/acp-19-15503-2019>
- Donohoe, A., Armour, K., Roe, G., Battisti, D., & Hahn, L. (2020). The partitioning of meridional heat transport from the last glacial maximum to CO₂ quadrupling in coupled climate models. *Journal of Climate*, 33(10), 4141–4165. <https://doi.org/10.1175/JCLI-D-19-0797.1>

- Funk, C., Hoell, A., Shukla, S., Husak, G., & Michaelsen, J. (2016). The east African monsoon system: Seasonal climatologies and recent variations. In L. M. V. de Carvalho & C. Jones (Eds.), *The monsoons and climate change: Observations and modeling* (pp. 163–185). Springer International Publishing. https://doi.org/10.1007/978-3-319-21650-8_8
- Gaetani, M., Messori, G., Zhang, Q., Flamant, C., & Pausata, F. S. R. (2017). 06). Understanding the mechanisms behind the northward extension of the West African monsoon during the mid-Holocene. *Journal of Climate*, *30*(19), 7621–7642. <https://doi.org/10.1175/JCLI-D-16-0299.1>
- Garellick, S., Russell, J., Richards, A., Smith, J., Kelly, M., Anderson, N., et al. (2022). The dynamics of warming during the last deglaciation in high-elevation regions of eastern equatorial Africa. *Quaternary Science Reviews*, *281*, 107416. <https://doi.org/10.1016/j.quascirev.2022.107416>
- Harrison, S. P., Bartlein, P. J., Brewer, S. C., Prentice, I. C., Boyd, M., Hessler, I., et al. (2014). Climate model benchmarking with glacial and mid-Holocene climates. *Climate Dynamics*, *43*(3–4), 671–688. <https://doi.org/10.1007/s00382-013-1922-6>
- Hopcroft, P. O., & Valdes, P. J. (2019). On the role of dust-climate feedbacks during the mid-Holocene. *Geophysical Research Letters*, *46*(3), 1612–1621. <https://doi.org/10.1029/2018GL080483>
- Hopcroft, P. O., & Valdes, P. J. (2021). Paleoclimate-conditioning reveals a north Africa land–atmosphere tipping point. *Proceedings of the National Academy of Sciences of the United States of America*, *118*(45), e2108783118. <https://doi.org/10.1073/pnas.2108783118>
- Hopcroft, P. O., Valdes, P. J., Harper, A. B., & Beerling, D. J. (2017). Multi vegetation model evaluation of the green Sahara climate regime. *Geophysical Research Letters*, *44*(13), 6804–6813. <https://doi.org/10.1002/2017GL073740>
- Hopcroft, P. O., Valdes, P. J., & Ingram, W. (2021). Using the mid-Holocene “greening” of the Sahara to narrow acceptable ranges on climate model parameters. *Geophysical Research Letters*, *48*(6), e2020GL092043. <https://doi.org/10.1029/2020GL092043>
- IPCC. (2013). Summary for policymakers [Book Section]. In T. Stocker, et al. (Eds.), *Climate change 2013: The physical science basis. contribution of working group I to the fifth assessment report of the intergovernmental panel on climate change* (pp. 1–30). Cambridge University Press. <https://doi.org/10.1017/CBO9781107415324.004>
- IPCC. (2021). Summary for policymakers. In V. Masson-Delmotte, et al. (Eds.), *Climate change 2021: The physical science basis. Contribution of working group I to the sixth assessment report of the intergovernmental panel on climate change* (pp. 3–32). Cambridge University Press. <https://doi.org/10.1017/9781009157896.001>
- Ivory, S. J., & Russell, J. (2016). Climate, herbivory, and fire controls on tropical African forest for the last 60ka. *Quaternary Science Reviews*, *148*, 101–114. <https://doi.org/10.1016/j.quascirev.2016.07.015>
- Izumi, K., Bartlein, P. J., & Harrison, S. P. (2015). Energy-balance mechanisms underlying consistent large-scale temperature responses in warm and cold climates. *Climate Dynamics*, *44*(11), 3111–3127. <https://doi.org/10.1007/s00382-014-2189-2>
- Jackson, M., Kelly, M., Russell, J., Doughty, A., Howley, J., Chipman, J., et al. (2020). Glacial fluctuations in tropical Africa during the last glacial termination and implications for tropical climate following the last glacial maximum. *Quaternary Science Reviews*, *243*, 106455. <https://doi.org/10.1016/j.quascirev.2020.106455>
- Joussaume, S., Taylor, K. E., Braconnot, P., Mitchell, J. F. B., Kutzbach, J. E., Harrison, S. P., et al. (1999). Monsoon changes for 6000 years ago: Results of 18 simulations from the paleoclimate modeling intercomparison project (PMIP). *Geophysical Research Letters*, *26*(7), 859–862. <https://doi.org/10.1029/1999GL900126>
- Kageyama, M., Albani, S., Braconnot, P., Harrison, S. P., Hopcroft, P. O., Ivanovic, R. F., et al. (2017). The PMIP4 contribution to CMIP6—Part 4: Scientific objectives and experimental design of the PMIP4-CMIP6 last glacial maximum experiments and PMIP4 sensitivity experiments. *Geoscientific Model Development*, *10*(11), 4035–4055. <https://doi.org/10.5194/gmd-10-4035-2017>
- Kaufman, D., & Broadman, E. (2023). Revisiting the Holocene global temperature conundrum. *Nature*, *614*(7948), 425–435. <https://doi.org/10.1038/s41586-022-05536-w>
- Kniffka, A., Knippertz, P., & Fink, A. H. (2019). The role of low-level clouds in the West African monsoon system. *Atmospheric Chemistry and Physics*, *19*(3), 1623–1647. <https://doi.org/10.5194/acp-19-1623-2019>
- Kok, J., Storelvmo, T., Karydis, V., Adebisi, A., Mahowald, N., Evan, A., et al. (2023). Mineral dust aerosol impacts on global climate and climate change. *Nature Reviews Earth & Environment*, *4*(2), 71–86. <https://doi.org/10.1038/s43017-022-00379-5>
- Linke, A. M., Witmer, F. D., O’Loughlin, J., McCabe, J. T., & Tir, J. (2018). Drought, local institutional contexts, and support for violence in Kenya. *Journal of Conflict Resolution*, *62*(7), 1544–1578. <https://doi.org/10.1177/0022002717698018>
- Liu, X., Battisti, D., & Donohoe, A. (2017). Tropical precipitation and cross-equatorial ocean heat transport during the mid-Holocene. *Journal of Climate*, *30*(10), 3529–3547. <https://doi.org/10.1175/JCLI-D-16-0502.1>
- Liu, Y., Zhang, M., Liu, Z., Xia, Y., Huang, Y., Peng, Y., & Zhu, J. (2018). A possible role of dust in resolving the Holocene temperature conundrum. *Scientific Reports*, *8*(1), 1–9. <https://doi.org/10.1038/s41598-018-22841-5>
- Liu, Z., Zhu, J., Rosenthal, Y., Zhang, X., Otto-Bliesner, B. L., Timmermann, A., et al. (2014). The Holocene temperature conundrum. *Proceedings of the National Academy of Sciences of the United States of America*, *111*(34), E3501–E3505. <https://doi.org/10.1073/pnas.1407229111>
- Loomis, S. E., Russell, J. M., & Lamb, H. F. (2015). Northeast African temperature variability since the late Pleistocene. *Palaeoecology, Palaeoecology*, *423*, 80–90. <https://doi.org/10.1016/j.palaeo.2015.02.005>
- Loomis, S. E., Russell, J. M., Verschuren, D., Morrill, C., De Cort, G., Damsté, J. S. S., et al. (2017). The tropical lapse rate steepened during the last glacial maximum. *Science Advances*, *3*(1), e1600815. <https://doi.org/10.1126/sciadv.1600815>
- McGee, D., Donohoe, A., Marshall, J., & Ferreira, D. (2014). Changes in ITCZ location and cross-equatorial heat transport at the last glacial maximum, Heinrich Stadial 1, and the mid-Holocene. *Earth and Planetary Science Letters*, *390*, 69–79. <https://doi.org/10.1016/j.epsl.2013.12.043>
- Meinshausen, M., Smith, S., Calvin, K., Daniel, J., Kainuma, M., Lamarque, J., et al. (2011). *The paleoclimate modeling intercomparison project contribution to CMIP5* (p. 15). WCRP Coupled Model Intercomparison Project-Phase 5-CMIP5.
- Morrissey, A., Scholz, C. A., & Russell, J. M. (2017). Late quaternary TEX86 paleotemperatures from the world’s largest desert lake, Lake Turkana, Kenya. *Journal of Paleolimnology*, *59*, 1–15. <https://doi.org/10.1007/s10933-016-9939-6>
- Nam, C., Bony, S., Dufresne, J.-L., & Chepfer, H. (2012). The ‘too few, too bright’ tropical low-cloud problem in CMIP5 models. *Geophysical Research Letters*, *39*(21), L21801. <https://doi.org/10.1029/2012GL053421>
- O’ishi, R., Chan, W.-L., Abe-Ouchi, A., Sherriff-Tadano, S., Ohgaito, R., & Yoshimori, M. (2021). PMIP4/CMIP6 last interglacial simulations using three different versions of MIROC: Importance of vegetation. *Climate of the Past*, *17*(1), 21–36. <https://doi.org/10.5194/cp-17-21-2021>
- Otto-Bliesner, B. L., Brady, E., Fasullo, J., Jahn, A., Landrum, L., Stevenson, S., et al. (2015). Climate variability and change since 850 C.E.: An ensemble approach with the community earth system model (CESM). *Bulletin of the American Meteorological Society*, *97*, 150807114607005. <https://doi.org/10.1175/BAMS-D-14-00233.1>

- Otto-Bliesner, B. L., Braconnot, P., Harrison, S. P., Lunt, D. J., Abe-Ouchi, A., Albani, S., et al. (2017). The PMIP4 contribution to CMIP6—Part 2: Two interglacials, scientific objective and experimental design for Holocene and last interglacial simulations. *Geoscientific Model Development*, 10(11), 3979–4003. <https://doi.org/10.5194/gmd-10-3979-2017>
- Pausata, F. S., Messori, G., & Zhang, Q. (2016). Impacts of dust reduction on the northward expansion of the African monsoon during the green Sahara period. *Earth and Planetary Science Letters*, 434, 298–307. <https://doi.org/10.1016/j.epsl.2015.11.049>
- Powers, L., Johnson, T. C., Werne, J. P., Castañeda, I. S., Hopmans, E. C., Sinninghe Damsté, J. S., & Schouten, S. (2005). Large temperature variability in the southern African tropics since the last glacial maximum. *Geophysical Research Letters*, 32(8), L08706. <https://doi.org/10.1029/2004GL022014>
- Ramos, R. D., LeGrande, A. N., Griffiths, M. L., Elsaesser, G. S., Litchmore, D. T., Tierney, J. E., et al. (2022). Constraining clouds and convective parameterizations in a climate model using paleoclimatic data. *Journal of Advances in Modeling Earth Systems*, 14(8), e2021MS002893. <https://doi.org/10.1029/2021MS002893>
- Rehfeld, K., & Laepple, T. (2016). Warmer and wetter or warmer and dryer? Observed versus simulated covariability of Holocene temperature and rainfall in Asia. *Earth and Planetary Science Letters*, 436, 1–9. <https://doi.org/10.1016/j.epsl.2015.12.020>
- Renssen, H., Brovkin, V., Fichefet, T., & Goosse, H. (2006). Simulation of the Holocene climate evolution in northern Africa: The termination of the African humid period. *Quaternary International*, 150(1), 95–102. (Impact of rapid environmental changes on humans and ecosystems). <https://doi.org/10.1016/j.quaint.2005.01.001>
- Sejas, S. A., & Cai, M. (2016). Isolating the temperature feedback loop and its effects on surface temperature. *Journal of the Atmospheric Sciences*, 73(8), 3287–3303. <https://doi.org/10.1175/JAS-D-15-0287.1>
- Shanahan, T., McKay, N., Hughen, K., Overpeck, J., Otto-Bliesner, B., Jr, C., et al. (2015). The time-transgressive termination of the African humid period. *Nature Geoscience*, 8(2), 140–144. <https://doi.org/10.1038/NNGEO2329>
- Sinninghe Damsté, J. S., Ossebaer, J., Schouten, S., & Verschuren, D. (2012). Distribution of tetraether lipids in the 25-ka sedimentary record of Lake Challa: Extracting reliable TEX86 and MBT/CBT palaeotemperatures from an equatorial African lake. *Quaternary Science Reviews*, 50, 43–54. <https://doi.org/10.1016/j.quascirev.2012.07.001>
- Stein, T. H. M., Parker, D. J., Hogan, R. J., Birch, C. E., Holloway, C. E., Lister, G. M. S., et al. (2015). The representation of the West African monsoon vertical cloud structure in the met office unified model: An evaluation with cloudsat. *Quarterly Journal of the Royal Meteorological Society*, 141(693), 3312–3324. <https://doi.org/10.1002/qj.2614>
- Sutton, R. T., Dong, B., & Gregory, J. M. (2007). Land/sea warming ratio in response to climate change: IPCC AR4 model results and comparison with observations. *Geophysical Research Letters*, 34(2), L02701. <https://doi.org/10.1029/2006GL028164>
- Thompson, A. J., Zhu, J., Poulsen, C., Tierney, J., & Skinner, C. (2022). Northern hemisphere vegetation change drives a Holocene thermal maximum. *Science Advances*, 8(15). <https://doi.org/10.1126/sciadv.abj6535>
- Thompson, A. J., Skinner, C. B., Poulsen, C. J., & Zhu, J. (2019). Modulation of mid-Holocene African rainfall by dust aerosol direct and indirect effects. *Geophysical Research Letters*, 46(7), 3917–3926. <https://doi.org/10.1029/2018GL081225>
- Tierney, J. E., Lewis, S. C., Cook, B. I., LeGrande, A. N., & Schmidt, G. A. (2011). Model, proxy and isotopic perspectives on the East African humid period. *Earth and Planetary Science Letters*, 307(1), 103–112. <https://doi.org/10.1016/j.epsl.2011.04.038>
- Tierney, J. E., Pausata, F. S., & de Menocal, P. B. (2017). Rainfall regimes of the green Sahara. *Science Advances*, 3(1), e1601503. <https://doi.org/10.1126/sciadv.1601503>
- Tierney, J. E., Poulsen, C. J., Montañez, I. P., Bhattacharya, T., Feng, R., Ford, H. L., et al. (2020). Past climates inform our future. *Science*, 370(6517), eaay3701. <https://doi.org/10.1126/science.aay3701>
- Tierney, J. E., Russell, J. M., Huang, Y., Damsté, J. S. S., Hopmans, E. C., & Cohen, A. S. (2008). Northern hemisphere controls on tropical southeast African climate during the past 60,000 years. *Science*, 322(5899), 252–255. <https://doi.org/10.1126/science.1160485>
- Tierney, J. E., & Tingley, M. P. (2015). A TEX86 surface sediment database and extended Bayesian calibration. *Scientific Data*, 2(1), 150029. <https://doi.org/10.1038/sdata.2015.29>
- Tierney, J. E., Ummenhofer, C. C., & de Menocal, P. B. (2015). Past and future rainfall in the horn of Africa. *Science Advances*, 1(9), e1500682. <https://doi.org/10.1126/sciadv.1500682>
- von Uexkull, N. (2014). Sustained drought, vulnerability and civil conflict in sub-Saharan Africa. *Political Geography*, 43, 16–26. <https://doi.org/10.1016/j.polgeo.2014.10.003>
- Williams, C. J. R., Guarino, M.-V., Capron, E., Malmierca-Vallet, I., Singarayer, J. S., Sime, L. C., et al. (2020). CMIP6/PMIP4 simulations of the mid-Holocene and last interglacial using HADGEM3: Comparison to the pre-industrial era, previous model versions and proxy data. *Climate of the Past*, 16(4), 1429–1450. <https://doi.org/10.5194/cp-16-1429-2020>
- Zelinka, M. D., Myers, T. A., McCoy, D. T., Po-Chedley, S., Caldwell, P. M., Ceppi, P., et al. (2020). Causes of higher climate sensitivity in CMIP6 models. *Geophysical Research Letters*, 47(1), e2019GL085782. <https://doi.org/10.1029/2019GL085782>
- Zhu, J., Liu, Z., Brady, E., Otto-Bliesner, B., Zhang, J., Noone, D., et al. (2017). Reduced ENSO variability at the LGM revealed by an isotope-enabled Earth system model. *Geophysical Research Letters*, 44(13), 6984–6992. <https://doi.org/10.1002/2017gl073406>
- Zhu, P., & Zhao, W. (2008). Parameterization of continental boundary layer clouds. *Journal of Geophysical Research*, 113(D10), D10201. <https://doi.org/10.1029/2007JD009315>

References From the Supporting Information

- Bao, Q., Lin, P., Zhou, T., Liu, Y., Yu, Y.-Q., Wu, G., et al. (2013). The flexible global ocean-atmosphere-land system model, spectral version 2: Fgoals-s2. *Advances in Atmospheric Sciences*, 30(3), 561–576. <https://doi.org/10.1007/s00376-012-2113-9>
- Bao, Q., Liu, Y., Wu, G., He, B., Li, J., Lei, W., et al. (2020). CAS FGOALS-f3-H and CAS FGOALS-f3-L outputs for the high-resolution model intercomparison project simulation of CMIP6. *Atmospheric and Oceanic Science Letters*, 13(6), 576–581. <https://doi.org/10.1080/16742834.2020.1814675>
- Berke, M. A., Johnson, T. C., Werne, J. P., Livingstone, D. A., Grice, K., Schouten, S., & Damsté, J. S. S. (2014). Characterization of the last deglacial transition in tropical East Africa: Insights from lake Albert. *Palaeogeography, Palaeoclimatology, Palaeoecology*, 409, 1–8. <https://doi.org/10.1016/j.palaeo.2014.04.014>
- Collins, W., Bellouin, N., Doutriaux-Boucher, M., Gedney, N., Halloran, P., Hinton, T., et al. (2011). Development and evaluation of an Earth-system model – HADGEM2. *Geoscientific Model Development Discussions*, 4, 1051–1075. <https://doi.org/10.5194/gmdd-4-997-2011>
- Gent, P. R., Danabasoglu, G., Donner, L. J., Holland, M. M., Hunke, E. C., Jayne, S. R., et al. (2011). The community climate system model version 4. *Journal of Climate*, 24(19), 4973–4991. <https://doi.org/10.1175/2011JCLI4083.1>

- Giorgetta, M. A., Jungclauss, J., Reick, C. H., Legutke, S., Bader, J., Böttinger, M., et al. (2013). Climate and carbon cycle changes from 1850 to 2100 in MPI-ESM simulations for the coupled model intercomparison project phase 5. *Journal of Advances in Modeling Earth Systems*, 5(3), 572–597. <https://doi.org/10.1002/jame.20038>
- Hajima, T., Watanabe, M., Yamamoto, A., Tatebe, H., Noguchi, M. A., Abe, M., et al. (2020). Development of the MIROC-ES2L Earth system model and the evaluation of biogeochemical processes and feedbacks. *Geoscientific Model Development*, 13(5), 2197–2244. <https://doi.org/10.5194/gmd-13-2197-2020>
- Jeffrey, S., Rotstayn, L., Collier, M., Dravitzki, S., Hamalainen, C., Moeseneder, C., et al. (2013). 03. Australia's cmip5 submission using the CSIRO-MK3.6 model. *Australian Meteorological and Oceanographic Journal*, 63, 1–13. <https://doi.org/10.22499/2.6301.001>
- Kageyama, M., Braconnot, P., Bopp, L., Caubel, A., Foujols, M.-A., Guilyardi, E., et al. (2012). Mid-Holocene and last glacial maximum climate simulations with the IPSL model—Part I: Comparing IPSL_CM5A TO IPSL_CM4. *Climate Dynamics*, 40(9–10), 1–22. <https://doi.org/10.1007/s00382-012-1488-8>
- Kelley, M., Schmidt, G. A., Nazarenko, L. S., Bauer, S. E., Ruedy, R., Russell, G. L., et al. (2020). GISS-E2.1: Configurations and climatology. *Journal of Advances in Modeling Earth Systems*, 12(8), e2019MS002025. <https://doi.org/10.1029/2019MS002025>
- Li, L., Lin, P., Yu, Y., Wang, B., Zhou, T., Liu, L., et al. (2013). The flexible global ocean-atmosphere-land system model, grid-point version 2: FGOALS-G2. *Advances in Atmospheric Sciences*, 30(3), 543–560. <https://www.proquest.com/scholarly-journals/flexible-global-ocean-atmosphere-land-system/docview/1328135260/se-2>
- Li, L., Yu, Y., Tang, Y., Lin, P., Xie, J., Song, M., et al. (2020). The flexible global ocean-atmosphere-land system model grid-point version 3 (FGOALS-G3): Description and evaluation. *Journal of Advances in Modeling Earth Systems*, 12(9), e2019MS002012. <https://doi.org/10.1029/2019MS002012>
- Mauritsen, T., & Roeckner, E. (2020). Tuning the MPI-ESM1.2 global climate model to improve the match with instrumental record warming by lowering its climate sensitivity. *Journal of Advances in Modeling Earth Systems*, 12(5), e2019MS002037. <https://doi.org/10.1029/2019MS002037>
- Schmidt, G. A., Kelley, M., Nazarenko, L., Ruedy, R., Russell, G. L., Aleinov, I., et al. (2014). Configuration and assessment of the GISS MODELE2 contributions to the CMIP5 archive. *Journal of Advances in Modeling Earth Systems*, 6(1), 141–184. <https://doi.org/10.1002/2013MS000265>
- Seland, Ø., Bentsen, M., Olivie, D., Toniazzo, T., Gjermundsen, A., Graff, L. S., et al. (2020). Overview of the Norwegian Earth system model (NORESM2) and key climate response of cmip6 deck, historical, and scenario simulations. *Geoscientific Model Development*, 13(12), 6165–6200. <https://doi.org/10.5194/gmd-13-6165-2020>
- Semmler, T., Danilov, S., Gierz, P., Goessling, H. F., Hegewald, J., Hinrichs, C., et al. (2020). Simulations for CMIP6 with the AWI climate model AWI-CM-1-1. *Journal of Advances in Modeling Earth Systems*, 12(9), e2019MS002009. <https://doi.org/10.1029/2019MS002009>
- Voldoire, A., Sanchez-Gomez, E., Salas y Méria, D., Decharme, B., Cassou, C., Sénési, S., et al. (2013). The CNRM-CM5.1 global climate model: Description and basic evaluation. *Climate Dynamics*, 40(9–10), 2091–2121. <https://doi.org/10.1007/S00382-011-1259-Y>
- Volodin, E., & Gritsun, A. (2018). Simulation of observed climate changes in 1850–2014 with climate model INM-CM5. *Earth System Dynamics*, 9(4), 1235–1242. <https://doi.org/10.5194/esd-9-1235-2018>
- Watanabe, S., Hajima, T., Sudo, K., Nagashima, T., Takemura, T., Okajima, H., et al. (2011). MIROC-ESM 2010: Model description and basic results of CMIP5-20C3M experiments. *Geoscientific Model Development*, 4(4), 845–872. <https://doi.org/10.5194/gmd-4-845-2011>
- Wu, T., Song, L., Li, W., Wang, Z., Zhang, H., Xin, X., et al. (2014). An overview of bcc climate system model development and application for climate change studies. *Acta Meteorologica Sinica*, 28(1), 34–56. <https://doi.org/10.1007/s13351-014-3041-7>
- Yukimoto, S., Adachi, Y., Hosaka, M., Sakami, T., Yoshimura, H., Hirabara, M., et al. (2012). A new global climate model of the meteorological research institute: MRI-CGCM3 model description and basic performance. *Journal of the Meteorological Society of Japan. Ser., II*(90A), 23–64. <https://doi.org/10.2151/jmsj.2012-A02>
- Yukimoto, S., Kawai, H., Koshiro, T., Oshima, N., Yoshida, K., Urakawa, S., et al. (2019). The meteorological research institute earth system model version 2.0, MRI-ESM2.0: Description and basic evaluation of the physical component. *Journal of the Meteorological Society of Japan*, 97(5), 931–965. <https://doi.org/10.2151/jmsj.2019-051>